

Benchmarking of Density Functionals for the Accurate Description of Thiol–Disulfide Exchange

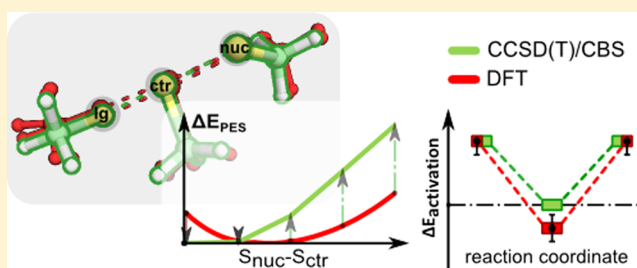
Rui P. P. Neves,[†] Pedro A. Fernandes,[†] António J. C. Varandas,[‡] and Maria J. Ramos^{*,†}

[†]REQUIMTE, Departamento de Química e Bioquímica, Faculdade de Ciências, Universidade do Porto, Rua do Campo Alegre, s/n, 4169-007 Porto, Portugal

[‡]Departamento de Química, and Centro de Química, Universidade de Coimbra, 3004-535 Coimbra, Portugal

S Supporting Information

ABSTRACT: A set of 92 density functionals was employed to accurately characterize thiol–disulfide exchange. The properties we have benchmarked throughout the study include the geometry of a 15 atoms model system, the potential energy surface, the activation barrier, and the energy of reaction for thiol–disulfide exchange. Reference energies were determined at the CCSD(T)/CBS//MP2/aug-cc-pVDZ level of theory, and reference geometries were calculated at the MP2/aug-cc-pVTZ level. M11-L, M06-2X, M06-HF, N12-SX, PBE1PBE, PBEh1PBE, and OHSE2PBE described better the geometry of the model system, with average deviations of 0.06 Å in bond lengths (0.06 Å in bond-breaking lengths) and 1.9° in bond angles. On the other hand, the potential energy surface and its gradient were more accurately described by the hybrid density functional BHandH, closely followed by mPW1N, mPW1K, and mPWB1K. The barrier height and energy of reaction were better reproduced by the BMK and M06-2X functionals (deviations of 0.17 and 0.07 kcal·mol⁻¹, respectively) for a set of 10 Pople's basis sets. MN12-SX and M11-L showed very good results for the widely used 6-311++G(2d,2p) basis set, with deviations of 0.02 and 0.05 kcal·mol⁻¹, respectively. We studied the effect of the split-valence, diffuse, and polarized functions in the activation barrier of thiol–disulfide exchange, for a set of 10 Pople's basis sets. While increasing the splitting and polarization may increase the activation barrier in approximately 1 kcal·mol⁻¹, diffuse functions generally contribute to decreasing it no more than 0.10 kcal·mol⁻¹. In general, 13 functionals provided energies within 1 kcal·mol⁻¹ of the reference value. The BB1K density functional is one of the best density functionals to characterize thiol–disulfide exchange reactions; however, several density functionals with modified Perdew–Wang exchange and about 40% Hartree–Fock exchange, such as mPW1K, mPW1N, and mPWB1K, show a good performance, too.

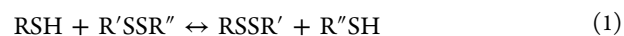


INTRODUCTION

Disulfide bonds are abundant in proteins.^{1–3} They are known to participate in some folding pathways and are part of the catalytic cycle of some enzymes. In cells, the thiol/disulfide ratio acts as a regulator of the cellular redox potential, it is involved in electron transfer processes across membranes and in the secreted proteins pathway.^{1,2,4,5} Atomistic insight of the involvement of these structures in cell regulation may, thus, result in rational pharmacological proceedings toward abnormalities in these processes.

The thiol/disulfide ratio in cells is mainly regulated by thiol–disulfide exchange and is generally assisted by the reduced glutathione/oxidized glutathione pair. Enzymes that perform thiol–disulfide exchange require an additional step to restart their catalytic cycles, for example, ribonucleotide, 3'-phosphoadenosine-5'-phosphosulfate (PAPS), or methionine sulfoxide reductases.¹ This step may be performed by a small molecule (e.g., glutathione) or by specialized enzymes. Disulfide oxidoreductases are the class of enzymes responsible for the formation, reduction, and isomerization of disulfide bonds, through thiol–disulfide exchange. This class of enzymes often

possess a characteristic Cys-X-X-Cys motif (being X any of the natural amino acids) and a considerable structural similarity to thioredoxin.⁴ Equation 1 shows the overall reaction for thiol–disulfide exchange.



This is usually a S_N2 reaction in which a cysteine or glutathione is being deprotonated and subsequently acting as a nucleophile, attacking the disulfide bond established by two cysteine (Cys) residues in a Cys-X-X-Cys motif. The attacking sulfur is usually named S_{nuc} (nucleophilic sulfur), the attacked sulfur is named S_{ctr} (central sulfur), and the sulfur that leaves the disulfide bond is named S_{ig} (leaving sulfur). The attack is driven along the disulfide bond axis and the reaction is expected to be intrinsically thermoneutral,^{6,7} even though the environment can provide different stabilities to S_{nuc} and S_{ig}, promoting the reaction toward one or another direction, depending on the physiological role of the specific enzyme. While in gaseous

Received: August 1, 2014

Published: September 29, 2014

phase the energy barrier of this reaction is inverted,^{6,8} in aqueous media the experimentally determined barrier is around 14 kcal·mol⁻¹.^{9,10} The transition state structure is approximately symmetrical relative to the attacked sulfur atom.^{6,8,11} The charge density delocalization through the three sulfur atoms in the transition state indicates that hydrophobic environments are better catalysts for the reaction.⁶ This evidence is also supported by pK_a studies in cysteines from the active site of disulfide oxidoreductases.¹²

Computational studies have been performed, regarding thiol–disulfide exchange using quantum mechanics calculations, in the recent past.^{8,13–15} Density Functional Theory (DFT)^{16–18} has been the preferred theoretical level when dealing with large chemical systems, even though there is no exchange–correlation approximation that consistently describes the energy of this interaction. The latter has been the target of several approaches over the past decades, from density functional (DF) development to correlated Hamiltonian methods.^{19–24} So far, in the DF field we have up to five main approximations for the description of the exchange–correlation energy: Local Density Approximation (LDA), Generalized Gradient Approximation (GGA), meta-Generalized Gradient Approximation (m-GGA), hybrid-Generalized Gradient Approximation (h-GGA), and hybrid-meta Generalized Gradient Approximation (hm-GGA). Other approximations to calculate this term have appeared in the recent years including the range-separated approach (rs),^{25–30} Nonseparable Gradient Approximation (NGA),^{31–33} and double-hybrid Generalized Gradient Approximation (hh-GGA).^{34–40}

Given the large number of DFs to calculate a given property of a chemical system, we must choose wisely. In the literature, we can find a plethora of benchmark studies to rank DFs for properties such as ionization and atomization energies, reaction energies, intermolecular and covalent interactions, proton and electron affinities, or structural parameters.^{41–44} Furthermore, several databases that compile specific reactions for chemical properties can be developed to test or rank any DF.^{45,46}

We provide here a study on DFT performance for thiol–disulfide exchange, in particular, the linkage and dissociation of disulfides by thiolate attack. To our knowledge, there are no recent benchmark studies for this reaction, even though it is prevalent in biochemistry.^{4,5,47,48} Our benchmarking is designed to rank the performance of DFs to reproduce structural and energy properties of this reaction, from the optimization of model systems to reaction coordinate linear transit scans, and ultimately providing accurate energies for the thiol–disulfide exchange reaction. Therefore, the main goals of our work are defined as (i) to provide a benchmarking on geometry accuracy on a representative model of the thiol–disulfide exchange reaction, (ii) to propose DFs to perform linear transit scans along the S_{nuc}–S_{ctr}–S_{lg} reaction coordinate, (iii) to determine a set of DFs that best describes the activation barrier and the energy of the thiol–disulfide exchange reaction. Our results are crossed with recent benchmark studies on several important chemical properties,^{41–43,46,49,50} to account for the wide spectra of chemical interactions that a complex medium possesses. The tests are performed with a group of basis sets ranging the double and triple split, polarized, and diffuse valence shells. We also test a number of range-separated DFs and several dispersion corrections.^{51–54}

To perform the benchmarking, we need reference values derived from accurate methods, such as coupled-cluster (CC)^{55,56} or configuration interaction (CI).^{20,21} These

methods require a high computational power and are currently restricted to small systems (less than 30 atoms), if using large basis sets. In this study, we performed single-point energy calculations, at the CCSD(T)^{22,55–60} level of theory, to determine CCSD(T)/CBS//MP2/aug-cc-pVDZ reference energies. We employ complete basis set (CBS) extrapolation methods^{61–65} to extrapolate both the Hartree–Fock (HF) and correlation energies.

■ COMPUTATIONAL METHODS

Model System. A 15 atom model system was built from thioredoxin glutathione reductase (PDB code: 2X8H) (Figure 1).⁶⁶ Thiol–disulfide exchange occurs through the nucleophilic

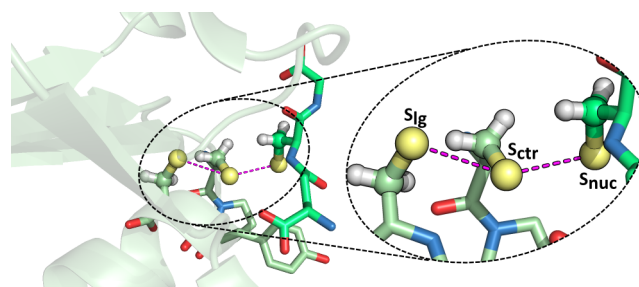


Figure 1. Enzyme thioredoxin glutathione reductase (2X8H) is shown in cartoon representation, with the Cys-X-X-Cys motif and the glutathione ligand in stick representation. Our model is highlighted by the black contour in the ball and stick representation. S_{lg}, S_{ctr}, and S_{nuc} stand for the leaving group, central, and nucleophilic sulfides, respectively.

attack of an external thiolate (mostly from glutathione) to the disulfide bond of the Cys-X-X-Cys motif. We have kept the terminal methylthiolate from glutathione (GSH1595) and the dimethyldisulfide from the Cys28-Pro29-Tyr30-Cys31 motif of thioredoxin reductase.

The computational procedure comprehends two stages, the *determination of reference structures and energies* and the *benchmarking of density functionals*. All the calculations were run with the Gaussian 09 software.⁶⁷

Reference Structures for Thiol–Disulfide Exchange.

We performed a linear transit scan in vacuum along the S_{nuc}–S_{ctr} distance at the MP2/aug-cc-pVDZ level of theory. The S_{nuc}–S_{ctr}–S_{lg} angle was constrained with three ghost atoms (Gh), by fixing Gh–S_{ctr}–S_{lg} and Gh–S_{nuc}–S_{ctr} angles (see Figure S1 in Supporting Information (SI)). These three ghost atoms establish a geometrical plane that constrains the S_{nuc}–S_{ctr}–S_{lg} angle to 180° throughout the potential energy surface (PES) calculation. This configuration is assumed as representative for a general nucleophilic attack. Ghost atoms have no charge or basis function information; therefore, they do not interfere in the quantum mechanical calculations. The PES has a parabolic shape, with only one stationary state (a minimum, the trisulfide anion). The minimum was reoptimized with MP2/aug-cc-pVTZ and served as reference geometry for the DF geometry benchmarking.

Reference Energies for Thiol–Disulfide Exchange. We performed geometry optimization calculations at the MP2 level of theory with the aug-cc-pVDZ basis set,^{68–70} in water, using the implicit conductor-like polarized continuum model (C-PCM)^{71,72} with a dielectric constant of 78.4. The reaction profile has shown three stationary points (R, TS, and P, Figure 2), whose electronic energy was recalculated, without the

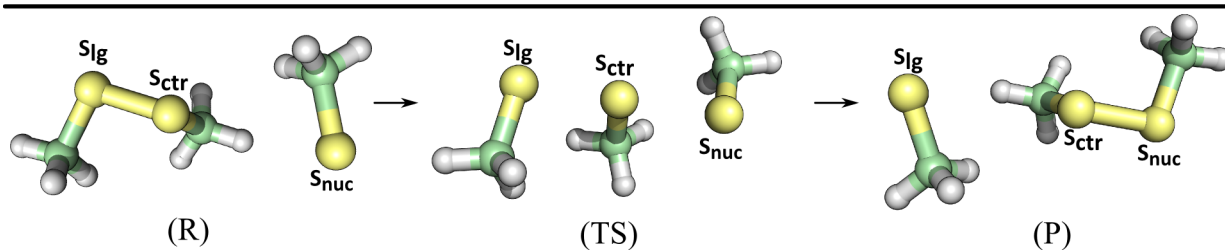


Figure 2. Reaction states for thiol–disulfide exchange, reagent (R), transition state (TS), and product (P), obtained at the MP2/aug-cc-pVDZ level of theory.

solvent, at the CCSD(T)/CBS//MP2/aug-cc-pVDZ level. The continuum solvent was taken out at the end to measure the errors from the functional only.

To investigate the PES shape in vacuum, we calculated the geometry and energy of a series of 20 increments of 0.010 Å, on both sides of the $S_{\text{nuc}}-S_{\text{ctr}}$ equilibrium bond length, at the MP2/aug-cc-pVDZ level of theory. We then used five equidistant steps, around the minimum of the PES, to calculate our reference PES. Such number of points was required to perform calculations at the CCSD(T)/CBS level.

We have employed the CBS extrapolation schemes for both the reaction energy profile and the $S_{\text{nuc}}-S_{\text{ctr}}$ relaxed PES (for further discussion, see Tables S4–S6 and Figure S4 in SI). We used energies from the MP2/aug-cc-pVXZ ($X = 2, 3, 4$) levels of theory to extrapolate for the MP2/CBS level, as recommended in the original schemes.^{61–65} CBS extrapolation schemes that use only the aug-cc-pVDZ and aug-cc-pVTZ basis sets may lead to inaccurate results,^{61,62,65} and calculations at the CCSD(T)/aug-cc-pVQZ level were too computationally demanding to be feasible. Therefore, we used the MP2/aug-cc-pVTZ and MP2/aug-cc-pVQZ single point energies to perform the CBS extrapolation for the correlation energy. We then determined the CCSD(T)/CBS energies, assuming that the differences in correlation energy between CCSD(T) and MP2 were the same when calculated using the aug-cc-pVTZ basis set or CBS (see the “CBS extrapolation schemes employed in the study” section, in SI).^{41,43,73–75} We did this for all stationary points of the reaction in water and for all points of the PES in vacuum. Despite the limitations that this approach might have, the final quality of the CCSD(T)/CBS energy is much superior to the DFT energies, and is adequate to be taken as a reference to benchmark the density functionals.

Geometry Benchmarking. Geometry optimizations were performed in vacuum, with the 92 density functionals employed in this study, for the 6-31G(d)^{76–81} and the 6-31+G(d)^{76–82} basis sets. These basis sets are frequently employed to optimize large biological systems, where the number of QM atoms usually ranges 100–300 atoms. To rank the performance of the set of DFs in geometry accuracy, we used the MP2/aug-cc-pVTZ optimized structure, in vacuum, as reference. We initially ranked our density functionals by root-mean-square deviation (RMSD) relatively to the reference structure. However, this criterion is insufficient, since it is an average measure of structure similarity and a more significant deviation in a given coordinate may pass unnoticed in the average. To avoid such situations, we checked for the most relevant internal coordinates and ranked separately (by RMSD) the functionals that did not violate either of the two premises that follow: (i) $S_{\text{nuc}}-S_{\text{ctr}}-S_{\text{lg}}$ angle deviations smaller than 3.0°; (ii) errors in any of the $S_{\text{nuc}}-S_{\text{ctr}}$, $S_{\text{ctr}}-S_{\text{lg}}$, and $S_{\text{nuc}}-S_{\text{lg}}$ distances no greater

than 0.1 Å. Among these, those with lower RMSD were considered to be more accurate. Even though the thresholds of 0.1 Å and 3.0° might seem arbitrary, in fact, results remain the same even if we change their value. A final note will be given on the threshold for bond lengths. A tenth of an Ångstrom seems to be too large an error for DFT, where common functionals have a bond length accuracy of about 0.01–0.03 Å. However, the potential energy surface along the sulfur–sulfur distance in the trisulfide anion in vacuum is extremely flat, allowing for bond elongations at a very modest energy cost.

Electronic Energy and PES Gradient Benchmarking. A set of 29 DFs, representative of the different exchange–correlation energy approximations and also based on the previous geometry benchmarking, were used to calculate the PES using the $S_{\text{nuc}}-S_{\text{ctr}}$ bond as the reaction coordinate, since it represents the nucleophilic attack of the cysteine to the glutathione ligand (see Figure 1). The PES for the 29 DFs were established with the 6-31G(d) basis set, which is the most common choice to perform PES calculations.^{8,14,83–88} We took into consideration also the popularity of some DFs (e.g. B3LYP).^{89–91} All comparisons of energies and gradients with the CBS data have been done using pure DFs and ab initio calculations, a point to emphasize since recent work^{92–94} has caution on the fact that “model chemistries” using hybrid methodologies may be misleading in describing the topography of the PESs described by the pure “chemistries” involved.

Single point energy calculations were carried out for the 92 DFs with 11 basis sets, namely 6-31+G(d,p),^{76–82} 6-31+G(2d,2p),^{76–82} 6-311G(d,p),^{78–81,95–97} 6-311G(2d,2p),^{78–81,95–97} 6-311G(2df,2p),^{78–81,95–97} 6-311G(2df,2pd),^{78–81,95–97} 6-311+G(df,p),^{78–82,95–97} 6-311++G(df,p),^{78–82,95–97} 6-311+G(2d,2p),^{78–82,95–97} 6-311++G(2d,2p),^{78–82,95–97} and TZVP,⁹⁸ to investigate the effect of valence splitting, polarization, and diffusion functions independently.

We checked the impact of the use of different integration grids, for three basis sets—6-311G(2df,2p), 6-311++G(df,p), and 6-311++G(2d,2p)—due to the sensitivity stated for some DFs, particularly the Minnesota family of functionals.⁹⁹ We used three pruned grids: the 75 302 default grid, the 99 590 grid, and the 150 974/225 974 grid. All deviations to the default pruned 75 302 grid are near 0.00 kcal·mol^{−1}. Exceptions stand for the M06-L (0.06 kcal·mol^{−1}), M06-2X, M06 (0.03 kcal·mol^{−1}), BMK (0.09 kcal·mol^{−1}), and ω B97X (0.04 kcal·mol^{−1}) functionals, for both the 99 590 and the 150 974/225 974 grids. The default grid seldom led to inaccuracies, and when they occur, they are very small (below 0.1 kcal·mol^{−1}). Additionally, we carried out single point energy calculations for the range separated version¹⁰⁰ of 34 pure DFs and 26 dispersion corrected DFs available in Gaussian 09. The parameters to

employ in Grimme's dispersion and with Becke–Johnson damping DFs were retrieved from Grimme's work.^{51–53} We employed a large number of the DFs to observe the differences of several DF approximations toward thiol–disulfide exchange, by introducing screened exchange or dispersion corrections.

RESULTS AND DISCUSSION

Characterization of Thiol–Disulfide Exchange. Figure 3 shows the PES profile for the HF, CCSD(T) correlation, and CCSD(T) electronic energies, extrapolated to the CBS limit, calculated for five relevant $S_{\text{nuc}}-S_{\text{ctr}}$ distances.

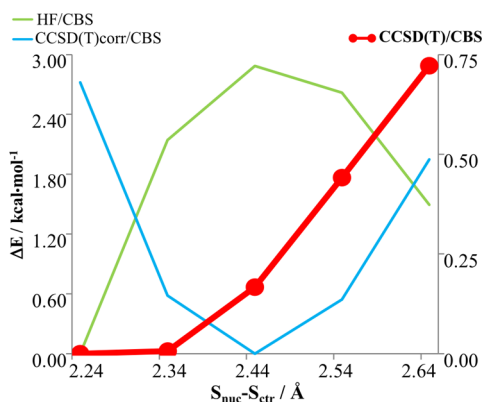


Figure 3. PES profile for the CBS extrapolated CCSD(T), HF, and CCSD(T)_{correlation} energies. The left axis corresponds to HF/CBS and CCSD(T)_{corr}/CBS energies, and to the right axis corresponds to the CCSD(T)/CBS energies obtained from Varandas' extrapolation scheme.

A minimum in the correlation energy can be observed when the three sulfur atoms are nearly equidistant ($S_{\text{lg}}-S_{\text{ctr}}$ and $S_{\text{ctr}}-S_{\text{nuc}}$ differ in 0.02 Å, see Figure 1) and the orbital overlap between the three sulfur atoms is maximum. For this same configuration, the HF energy is at a maximum, since the electron–electron repulsion due to orbital overlapping is high. We observe also that a $S_{\text{nuc}}-S_{\text{ctr}}$ stretch of 0.20 Å leads to energy differences up to 3 kcal·mol⁻¹ and completely different energy profiles at the HF and CCSD(T) levels of theory. Figure 3 exemplifies quite well how strongly the correlation energy influences the geometry and energy for our thiol–disulfide exchange model. Therefore, the careful choice of an adequate density functional is necessary and fully justified.

Our calculations performed in vacuum failed to provide a local minima representative of the configuration expected in an enzymatic environment, since in X-ray structures of enzymes the thiolate anion is either in an oxidized or reduced form; hence, we performed calculations with implicit aqueous solvent (C-PCM), which provided closer results to the observed in X-ray structures. Figure 4 shows the energy profile obtained from the CBS extrapolation scheme of Varandas, for both vacuum and aqueous implicit solvent.

Table 1 presents the energy of the TS (relative to the R), in vacuum ($\Delta E_{\text{PES depth}}$) and implicit water C-PCM ($\Delta E_{\text{activation}}$), obtained at the MP2/aug-cc-pVXZ ($X = 2-4$), CCSD(T)/aug-cc-pVXZ ($X = 2, 3$), and CBS extrapolated levels of theory.

Comparing the MP2/aug-cc-pVXZ and the MP2/CBS energies to the CCSD(T)/aug-cc-pVXZ and CCSD(T)/CBS energies, one can observe that MP2 energies converge faster toward the CBS limit with the increase of the basis set size. The CCSD(T)/CBS results show an activation energy of 9.61 kcal·

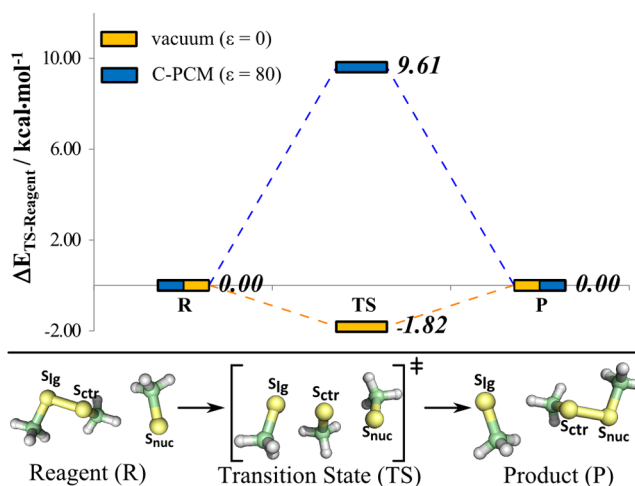


Figure 4. Energy profile for the thiol–disulfide reaction obtained with the CBS extrapolation scheme of Varandas, for the vacuum and implicit solvation models, using the geometries optimized in solvent.

Table 1. Electronic Energies from Single-Point Calculations for the R, TS, and P States with MP2 and CCSD(T) Methods, and CBS Extrapolation^a

method/basis set	$\Delta E_{\text{PES depth}}$ (kcal·mol ⁻¹) (vacuum)	$\Delta E_{\text{activation}}$ (kcal·mol ⁻¹) (water)
$E_{\text{MP2/DZ}}$	-5.05	6.24
$E_{\text{MP2/TZ}}$	-4.38	7.05
$E_{\text{MP2/QZ}}$	-4.09	7.36
$E_{\text{MP2/CBS}}$	-4.06	7.38
$E_{\text{CCSD(T)/DZ}}$	-3.31	7.90
$E_{\text{CCSD(T)/TZ}}$	-2.13	9.28
$E_{\text{CCSD(T)/CBS}}$	-1.82	9.61

^aDZ stands for the aug-cc-pVDZ basis set, TZ stands for the aug-cc-pVTZ basis set, and QZ stands for the aug-cc-pVQZ basis set.

mol⁻¹, different from the 14 kcal·mol⁻¹ experimental estimate in the literature.^{9,10} Our calculations have used an implicit solvent model (with well-known limitations) and do not include entropic or zero point energy (ZPE) corrections. We estimated the ZPE and thermal free energy corrections in 8.05 kcal·mol⁻¹, from MP2/aug-cc-pVDZ calculations.

Benchmarking Geometry of the Thiol–Disulfide Exchange Model. Since disulfide crossed-links have been described as strongly relying in the method employed,¹⁰¹ we have benchmarked the quality of the molecular geometry, in vacuum, with the 6-31G(d) and 6-31+G(d) basis sets, against the MP2/aug-cc-pVTZ optimized structure.

These basis sets are representative of this type of calculations in large systems and are extensively used in computational chemistry. Larger basis sets could be employed here but would not be of practical use in studies of applications to realistic biological systems. Of course, the criticism may be that any good agreement with a small basis set may just be accidental, an argument that we cannot unfortunately counterargue. However, we are interested in interaction energies, and hence, such considerations may not have drastic implications. Table 2 shows the DFs that have fulfilled the criteria that we established in the methods section (further results can be found in SI, Tables S24 and S25). Overall, the average error in bond lengths is slightly above of what is typically expected from DFT methods (generally below 0.05 Å),^{44,102,103} which is due to the

Table 2. Best Performing Density Functionals for the 6-31G(d) and the 6-31+G(d) Basis Sets^a

	$S_{\text{ctr}}-S_{\text{lg}}$ (Å)	$S_{\text{ctr}}-S_{\text{nuc}}$ (Å)	$S_{\text{lg}}-S_{\text{ctr}}-S_{\text{nuc}}$ (deg)	$(S_{\text{ctr}}-S_{\text{lg}})-(S_{\text{ctr}}-S_{\text{nuc}})$ (Å)	MUE (Å)	RMS (Å)
MP2/aug-cc-pVTZ	2.42	2.40	179.8	0.02		
			6-31G(d)			
M11-L	0.08	0.06	-2.0	0.04	0.06	0.43
PW91B95	0.10	0.09	-0.5	0.03	0.07	0.44
PBEB95	0.10	0.10	-0.7	0.03	0.08	0.44
SVWN	0.03	0.02	-0.5	0.02	0.02	0.45
SVWN5	0.03	0.03	-0.3	0.02	0.03	0.45
MN12-SX	0.08	0.06	-0.8	0.04	0.06	0.45
M06-2X	0.07	0.03	-0.4	0.05	0.05	0.45
M06	0.08	0.04	-1.3	0.06	0.06	0.45
M06-HF	0.04	0.03	-0.2	0.03	0.03	0.46
DSD-BLYP	0.08	0.06	-2.1	0.03	0.06	0.47
N12-SX	0.05	0.02	-2.1	0.04	0.04	0.47
B2GPPLYP	0.08	0.06	-2.3	0.04	0.06	0.47
mPW2PLYP	0.09	0.07	-2.4	0.04	0.07	0.47
mPW1B95	0.10	0.10	-2.2	0.02	0.07	0.48
mPWB95	0.10	0.10	-2.2	0.02	0.07	0.48
PBE1PBE	0.06	0.04	-2.5	0.04	0.05	0.48
B2PLYP	0.09	0.08	-2.7	0.04	0.07	0.48
PBEh1PBE	0.07	0.04	-2.5	0.05	0.05	0.48
OHSE2PBE	0.07	0.04	-2.6	0.05	0.05	0.48
mPW1PBE	0.07	0.04	-2.8	0.04	0.05	0.49
mPW1PW91	0.07	0.04	-2.8	0.04	0.05	0.49
APF	0.07	0.05	-2.8	0.04	0.05	0.49
TPSSh	0.10	0.08	-2.3	0.03	0.07	0.50
B3P86	0.07	0.05	-2.9	0.04	0.05	0.50
TPSS1KCIS	0.10	0.08	-2.8	0.04	0.07	0.50
...
B3LYP	0.07	0.04	-3.4	0.05	0.05	0.51
			6-31+G(d)			
M11-L	0.02	0.09	-2.6	-0.05	0.05	0.44
M062-X	-0.01	0.10	-0.9	-0.09	0.07	0.45
SVWN	0.00	0.04	-0.3	-0.02	0.02	0.46
SVWN5	0.01	0.04	-0.5	-0.02	0.02	0.46
M06-HF	0.01	0.06	-0.6	-0.03	0.03	0.47
N12-SX	0.00	0.06	-2.6	-0.04	0.03	0.48
PBEh1PBE	0.01	0.08	-2.8	-0.05	0.05	0.48
PBE1PBE	0.01	0.08	-2.9	-0.05	0.05	0.48
OHSE2PBE	0.02	0.08	-2.9	-0.05	0.05	0.48
...
B3LYP	0.02	0.09	-3.9	0.05	0.05	0.52

^aThe first four columns show the unsigned error with respect to the reference values for the tested DFs. The MUE refers to the mean unsigned average error of the $S_{\text{ctr}}-S_{\text{lg}}$, $S_{\text{ctr}}-S_{\text{nuc}}$ and $(S_{\text{nuc}}-S_{\text{ctr}})-(S_{\text{lg}}-S_{\text{ctr}})$ lengths.

unusual flatness of the PES of this system for the sulfur–sulfur distance. As verified in a paper by Goerigk and Reimers,¹⁰¹ geometries obtained with double-split valence basis sets predominantly overestimate sulfur–sulfur stretching, relatively to the MP2/aug-cc-pVTZ structure. Among the best performing DFs, m-GGAs show the highest deviations to the reference values and increasing inclusion of HF exchange shortens these differences.

The Minnesota functionals, M11-L, M06-2X, M06-HF, and N12-SX, along with PBE1PBE, PBEh1PBE, and OHSE2PBE show the best performance for the set of two basis sets tested. We remark the less good performance of the range separated DFs. B3LYP was not among the best functionals; nevertheless, it showed a similar performance for both 6-31G(d) and 6-31+G(d) basis sets (ranked 60th and 48th, respectively), with RMSD of 0.51 and 0.52 Å for this system.

The five hh-GGA DFs show good performance with the 6-31G(d) basis set. However, with the 6-31+G(d) basis set they were unable to reproduce the similarity in the $S_{\text{ctr}}-S_{\text{lg}}$ and $S_{\text{ctr}}-S_{\text{nuc}}$ bonds exhibited by the reference structure. Other works have already shown that hh-GGAs do not present good results when double-split valence basis sets are employed;^{35,42,104} therefore, employing hh-GGAs to obtain molecular geometries is limited to smaller systems and may not be adequate to carry out QM calculations in biological systems, where the size of the system must be considerable to account for the most significant interactions in the chemical environment.

A final remark on the set of DFs employed: some current works highlight the role of dispersion as well as basis set error corrections to accurately describe both the system's energy and structure,^{42,101,105–107} in particular, when small basis sets, such as 6-31G(d), empirical long-range dispersion, and basis set

Table 3. MUEs, in kcal·mol⁻¹, for a Set of 29 DFs Used to Determine the PES from CCSD(T)/CBS Calculations (See Figure 4)^a

$S_{\text{ctr}}-S_{\text{nuc}}$ (Å)		2.25	2.35	2.45	2.55	2.65		
ΔE (kcal·mol ⁻¹)		0.00	0.01	0.17	0.44	0.72		
DF	E_{xc}	% E_{x}^{HF}	error (kcal·mol ⁻¹)				MUE (kcal·mol ⁻¹)	
SVWN	LDA		1.21	0.19	-0.15	-0.02	0.54	0.42
HCTH407	GGA		0.97	0.32	-0.13	-0.42	-0.51	0.47
PBE	GGA		2.04	0.67	-0.09	-0.40	-0.30	0.70
BP86	GGA		2.08	0.70	-0.08	-0.41	-0.33	0.72
PW91	GGA		2.11	0.75	-0.05	-0.42	-0.39	0.75
BLYP	GGA		2.84	1.21	0.17	-0.43	-0.61	1.05
M11-L	m-GGA		0.79	0.20	-0.16	-0.35	-0.34	0.37
VSXC	m-GGA		1.43	0.52	-0.07	-0.43	-0.50	0.59
PW91TPSS	m-GGA		1.87	0.59	-0.11	-0.38	-0.26	0.64
TPSS	m-GGA		2.05	0.71	-0.07	-0.41	-0.35	0.72
BHandH	h-GGA	50.00	0.09	0.00	-0.11	-0.26	-0.29	0.15
mPW1N	h-GGA	40.60	0.24	0.02	-0.15	-0.30	-0.34	0.21
mPW1K	h-GGA	42.80	0.20	0.01	-0.15	-0.33	-0.40	0.22
PBE1PBE	h-GGA	25.00	0.81	0.17	-0.17	-0.28	-0.15	0.31
mPW1PBE	h-GGA	25.00	0.83	0.18	-0.17	-0.29	-0.17	0.33
mPW1PW91	h-GGA	25.00	0.84	0.18	-0.17	-0.30	-0.19	0.34
B3LYP	h-GGA	20.00	1.34	0.44	-0.12	-0.41	-0.43	0.54
mPWB1K	hm-GGA	44.00	0.11	-0.01	-0.13	-0.30	-0.39	0.19
BB1K	hm-GGA	42.00	0.18	0.01	-0.15	-0.34	-0.42	0.22
M06-2X	hm-GGA	54.00	0.64	0.12	-0.16	-0.26	-0.16	0.27
M06-HF	hm-GGA	100.00	0.77	0.13	-0.16	-0.23	-0.06	0.27
BMK	hm-GGA	42.00	0.31	0.00	-0.14	-0.34	-0.57	0.27
N12-SX	h-NGA	25.00/- ^b	0.77	0.13	-0.16	-0.23	-0.06	0.27
MN12-L	m-NGA		0.30	0.04	-0.16	-0.39	-0.54	0.29
MN12-SX	hm-NGA	25.00/- ^b	0.64	0.15	-0.17	-0.35	-0.34	0.33
N12	NGA		0.80	0.14	-0.16	-0.25	0.73	0.42
B2GPPLYP	hh-GGA	53.00	0.67	0.17	0.00	-0.08	-0.36	0.35
DSD-BLYP	hh-GGA	65.00	0.72	0.20	-0.01	-0.08	-0.39	0.36
B2PLYP	hh-GGA	70.00	1.02	0.30	-0.02	-0.06	-0.36	0.44

^aAll DFT calculations were performed with the 6-31G(d) basis set. ^bScreened HF exchange at short and long ranges.

error considerations have led to significant improvement in molecular geometry, particularly, when conformers of the molecular PES show very low barriers.^{101,107} Nevertheless, as larger environments are treated, these empirical corrections may be required to obtain either more accurate geometries or energies. Our study did not account for such corrections since we used a small model, based on the fact that we carried out extensive work on the thioresoxin family of enzymes,^{6,13,108–111} which employs the reactive system of thiol–disulfide exchange for catalysis. Most of our past studies on these enzymes have been performed on such small systems, but the results⁶ have been validated by single-molecule force spectroscopy.^{112–114}

Benchmarking the PES along the Reaction Coordinate. Table 3 shows the average MUEs for the five equidistant CCSD(T)/CBS energies in the $S_{\text{ctr}}-S_{\text{nuc}}$ linear transit scan, for a set of 29 functionals. We have used the 6-31G(d) basis set because it is with this basis set (or with basis sets of similar size) that the PES is frequently explored for systems of considerable size. Therefore, this study does not present the accuracy of functionals in terms of electronic energy but instead the accuracy with which they generate the PESs. These DFs were chosen to cover the several existing families and were based on the geometry benchmarking presented beforehand.

Our results show that density functionals, with little or no HF exchange, do not reproduce accurately the CCSD(T)/CBS reference energies for the several $S_{\text{ctr}}-S_{\text{nuc}}$ distances in the PES

or the overall interaction. Hybrid functionals with 40–50% HF exchange and the modified Perdew and Wang exchange^{115–120} have shown good accuracy in describing the thiol–disulfide exchange energies (see also single-point calculations for the $\Delta E_{\text{PES depth}}$ in SI). This percentage of HF exchange has been described in previous studies to be needed to accurately describe barrier heights.^{121–123} In general, pure DFs show the highest MUE among the set of DFs tested. Among the several DF approximations, the hm-GGA set of DFs consistently describes the energies for the five points of the PES with the lowest errors, all rounding 0.20–0.30 kcal·mol⁻¹. For the hh-GGA set of DFs, we observe increasing MUE values as the percentage of HF exchange increases. B3LYP gives relative energies higher than the reference energies when the $S_{\text{ctr}}-S_{\text{nuc}}$ distance is lower than 2.45 Å. However, the same is observed for almost all other DFs tested. Overall, the BHandH, mPW1N, mPW1K, mPWB1K, and BB1K functionals show a good and similar performance for energy calculations. We notice that again the functional BB1K stands out as one of the best.

An energy analysis from our set of DFs is not enough to choose those that best represent the PES energy for thiol–disulfide exchange. The adequate functional must be accurate in both energy and energy gradient toward the CCSD(T)/CBS PES. Indeed, the fact that the CCSD(T)/CBS and the DFT/6-31G(d) curves must be parallel is key to certify similar dynamical attributes for the density functional performance.

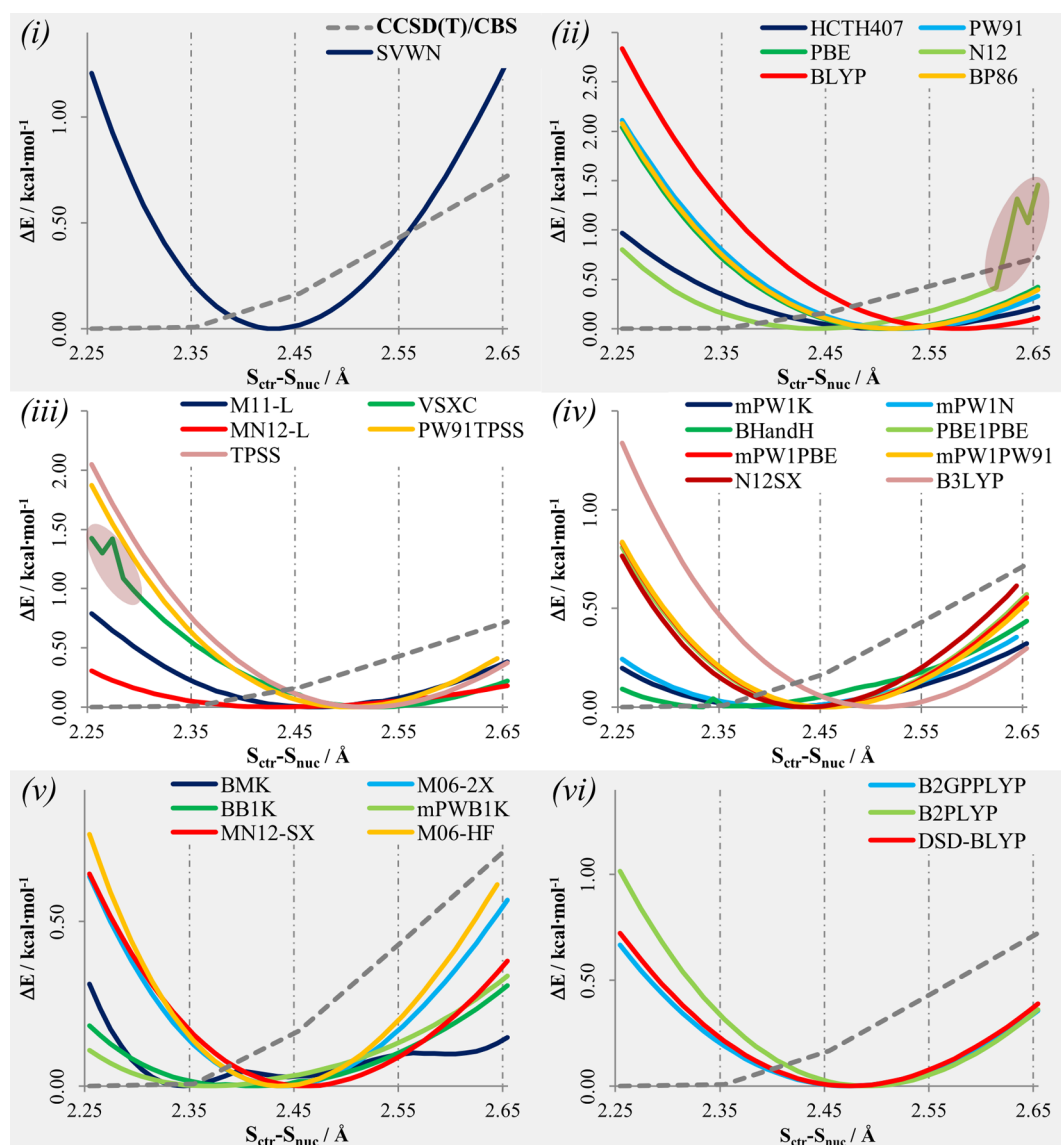


Figure 5. Comparison of the PES scans for the selected functionals with the 6-31G(d) basis set, and the reference PES from CCSD(T)/CBS calculations. We analyze DF performance according to E_{xc} approximation for each set: (i) LDA, (ii) GGA, and NGA, (iii) m-GGA and m-NGA, (iv) h-GGA and h-NGA, (v) hm-GGA and hm-NGA, and (vi) hh-GGA. The CCSD(T)/CBS calculated PES is shown with gray dashes.

Our analysis turns now to the energy gradient along the $S_{ctr}-S_{nuc}$ reaction coordinate, where we compare four equidistant intervals from the CCSD(T)/CBS PES of the reaction coordinate. Figure 5 shows our results for the several approaches to the exchange-correlation (E_{xc}) term. We performed a comparison of the energy gradient as we go farther from the equilibrium distance of the PES. In this way, we evaluate both the energy and energy gradient accuracies, toward the CCSD(T)/CBS PES, taking into account that new geometries are being obtained from the DF itself.

An overall look at Figure 5 shows that no DF reproduces accurately the energy gradient of the reference PES, which we observe to be very flat. We also notice that the energy minimum from the PES of each density functional does not seem to be moving close to the 2.25–2.35 Å distance.

Regarding the GGA functionals, we observe that the energy minimum is shifted toward larger $S_{ctr}-S_{nuc}$ values, relatively to the reference PES; however, the energy gradient toward larger values of $S_{ctr}-S_{nuc}$ seems to agree with the gradient estimated

by our extrapolated PES for the PW91, PBE, and BP86 functionals. Comparatively to the GGA approximation, the introduction of kinetic spin interaction in the Hamiltonian improves the PES obtained from m-GGAs. The M11-L functional, followed by MN12-L, shows the best performance in reproducing the CCSD(T)/CBS PES for the thiol–disulfide exchange reaction in this class of DFs. The N12 density functional shows a discontinuous behavior farther from the 2.60 Å distance and VSXC presents a slight discontinuity for values of $S_{ctr}-S_{nuc}$ close to 2.30 Å, hence these regions were considered in this part of our discussion.

Analyzing the h-GGA class of functionals, we can observe a clear dependence on energy profile and HF exchange. DFs with 25% HF exchange (PBE1PBE, mPW1PBE, and mPW1PW91) show an identical behavior, closely followed by the N12-SX functional. The BHandH, mPW1N, and mPW1K functionals, with 40–50% HF exchange, show the lowest energy deviations. BHandH shows the closest results to the CCSD(T)/CBS extrapolated PES in both energy accuracy and energy gradient.

We emphasize, particularly, the performance of B3LYP due to its high popularity. It overestimates the energy for short $S_{\text{ctr}}-S_{\text{nuc}}$ distances and the energy gradient profile along the reaction coordinate becomes more consistent with the CCSD(T)/CBS profile for values larger than the equilibrium distance (see Figure 5). The results from the hm-GGA class of DFs do not differ substantially from h-GGA DFs, with the mPWb1K and BB1K functionals showing the best overall performance. While the BMK functional performs accurate energy calculations for the reaction coordinate, comparatively to the CCSD(T)/CBS PES, the kinetics of the $S_{\text{ctr}}-S_{\text{nuc}}$ bond throughout the linear transit scan failed to be reproduced.

B2PLYP, B2GPPLYP, and DSD-LYP functionals, all hh-GGAs, behaved similarly in this part of the study. Despite none of them being able to accurately describe the PES gradient at the CCSD(T)/CBS level of theory, MUEs were relatively small comparatively to the CCSD(T)/CBS PES (in the 0.30–0.40 kcal·mol⁻¹ range). This gradient is more similar between these DFs, as we move for larger $S_{\text{ctr}}-S_{\text{nuc}}$ distances.

Benchmarking of the Activation Energy for Thiol–Disulfide Exchange. A set of 92 DFs^{18,25–40,89–91,100,115–122,124–166} was benchmarked against CCSD(T)/CBS activation energies. All calculations show the overall reaction to be thermoneutral, with errors often lower than 0.1 kcal·mol⁻¹.

LDA DFs present the less exact activation energy ($\Delta E_{\text{PES depth}}$) for thiol–disulfide exchange, with errors around 10 kcal·mol⁻¹ for any of the 11 basis sets tested, while B3LYP shows errors within the 3 kcal·mol⁻¹ underestimation error attributed to this density functional. This has been observed also for several other properties in other benchmark studies.^{41–43} In Table 4, we show the set of density functionals

Table 4. Set of DFs, within the 1 kcal·mol⁻¹ Error from the Reference Value for the 6-311++G(2d,2p) Basis Set^a

method/basis set		$\Delta E_{\text{PES depth}}$ (kcal·mol ⁻¹)	
CCSD(T)/CBS		–1.82	
DF	$E_{\text{xc}}[\rho]$	% E_{x}^{HF}	error
OVWN5	GGA		–0.21
OPL	GGA		–0.27
OVWN	GGA		–0.48
M11-L	m-GGA		–0.05
mPW1K	h-GGA	42.80	0.14
mPW1N	h-GGA	40.60	–0.23
BMK	hm-GGA	42.00	0.11
M06-2X	hm-GGA	54.00	–0.29
BB1K	hm-GGA	42.00	0.46
mPWB1K	hm-GGA	44.00	0.57
mPWK1S1K	hm-GGA	41.00	0.95
MN12-L	m-NGA		0.43
MN12-SX	hm-NGA	25.00/ ^b	0.02

^aThe DFs are displayed by exchange correlation energy (E_{xc}) approximation and increasing error. ^bScreened HF exchange at short- and long-range.

that performed better (within 1.00 kcal·mol⁻¹) for the 6-311++G(2d,2p) basis set, which is commonly used in single-point calculations in mechanistic studies.^{83–86} The Minnesota family of DFs shows good performance toward the reaction we have studied, as there are 4 of these density functionals that show an error smaller than 1 kcal·mol⁻¹ from the CCSD(T)/CBS values, in 10 of the tested DFs. The results for the whole 92

density functionals are given in SI (see Table S7). An error of 1 kcal·mol⁻¹ might seem large in sight of the magnitude of the interaction and reaction energies of thiol–disulfide exchange. However, this is illusory, since the activation and reaction energies are differences between large numbers, and if they are not accurate, the differences may take large positive/negative values. Hence, to calculate a relative error does not make sense here because the limits of the scale are not determined.

We tested the systematic behavior of the 92 DFs with basis sets having different valence splitting, polarization, and diffuse Gaussian functions and show in Figure 6 the results for a set of 17 DFs that performed within 1.00 kcal·mol⁻¹ for at least half of the 10 Pople's basis sets tested and B3LYP.^{89–91} The objective of the next part of our discussion is not to choose the best basis set to approach with a given functional, but instead, we try to give insight on the confidence the user can get from selecting a given DF to study the thiol–disulfide exchange reaction.

We observe that inclusion of diffuse basis sets in heavy atoms decreases the $\Delta E_{\text{PES depth}}$ for most density functionals, in about 0.10 kcal·mol⁻¹, relative to the 6-311G(2d,2p) energy. As we introduce diffuse functions in hydrogen atoms, we notice that errors from the reference energy are nearly the same (see dark gray bars in Figure 6). The cases in which this deviation is larger are observed for h-GGA DFs with high HF exchange (higher than 40%).

Comparing the energy calculations from the double and triple-split valence basis sets, we observe that the $\Delta E_{\text{PES depth}}$ decreases for almost all density functionals (see white bars in Figure 6). These decrements are always smaller than 1 kcal·mol⁻¹. Only for M11-L¹⁶⁶ and M06-HF,^{160,161} larger split-valence leads to a higher $\Delta E_{\text{PES depth}}$. The m-GGA and hh-GGA sets of DFs show the largest standard deviations.

The effect of increasing polarization can be observed in light gray bars in Figure 6. This property shows the highest variation in the thiol–disulfide exchange reaction. Figure 6 shows that increasing polarization leads to higher $\Delta E_{\text{PES depth}}$, as we approach the 6-311G(d,p), 6-311G(2d,2p), and 6-311G-(2df,2pd) basis sets. Differences in $\Delta E_{\text{PES depth}}$ among these basis sets, can be larger than 1.00 kcal·mol⁻¹, although that was only observed for 6 DFs. In general, as polarization increases the $\Delta E_{\text{PES depth}}$ obtained for each DF increases in a nonlinear manner. The exception stands for the hh-GGA set of DFs. In this latter set, we observe a decrease in the PES depth from 6 to 311G(d,p) to 6-311G(2d,2p), and an increase from the 6-311G(2d,2p) to 6-311G(2df,2pd) basis sets. The $\Delta E_{\text{PES depth}}$ for the 6-311G(2d,2p) basis set are the farthest from the reference value. Density functionals from the m-GGA set show more equally spaced $\Delta E_{\text{PES depth}}$ deviations (see Table S21 in SI). The m-GGA and hm-GGA set of DFs provide larger $\Delta E_{\text{PES depth}}$ for highly polarized basis sets; the latter show nonlinear variations of $\Delta E_{\text{PES depth}}$ with increasing polarization—introduction of f and d orbitals in heavy and hydrogen atoms, respectively, shows a higher increase in $\Delta E_{\text{PES depth}}$ for the thiol–disulfide exchange.

The choice of basis set is of utmost importance in any DFT energy calculation. As a general conclusion, we tentatively propose that the combination of triple-valence basis sets with highly polarized functions and diffuse orbitals in heavy atoms should be employed in the thiol–disulfide exchange.

Additionally, we have tested density functionals with screened HF exchange terms or dispersion corrections for three basis sets out of the 11 used. Density functionals with screened HF exchange show no improvement relatively to pure

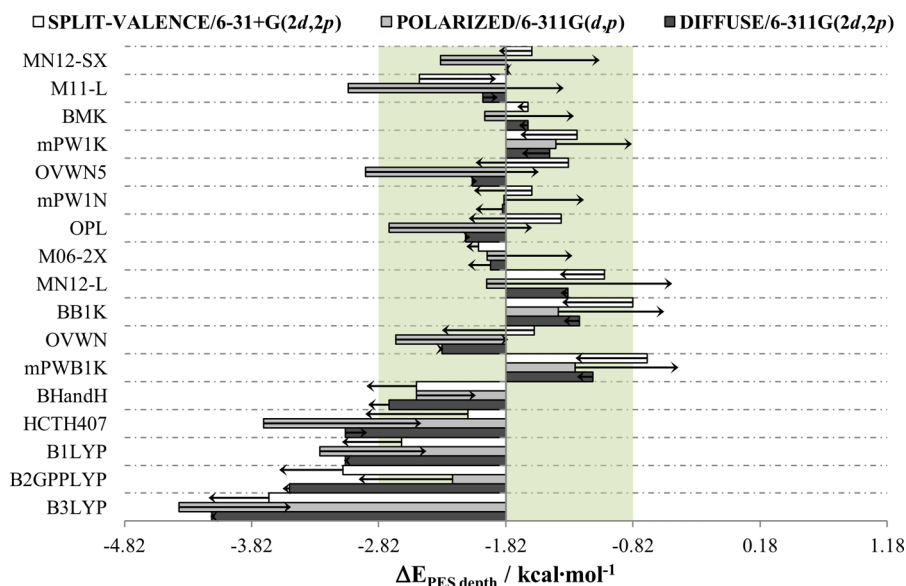


Figure 6. Effect of splitting, polarization, and diffuse functions in the DF energies. The bars represent the energy determined with the smaller basis set and the arrows show the mean basis set truncation error obtained with larger basis sets in relation to the smaller basis set. The green region marks the limiting error of $1.00 \text{ kcal}\cdot\text{mol}^{-1}$.

DFs, as can be seen in Figure 7. Contrary to pure DFs, which underestimate the reference activation energy, we observe that the activation energy is constantly overestimated over the CCSD(T)/CBS energy, except for M11-L, in which deviations

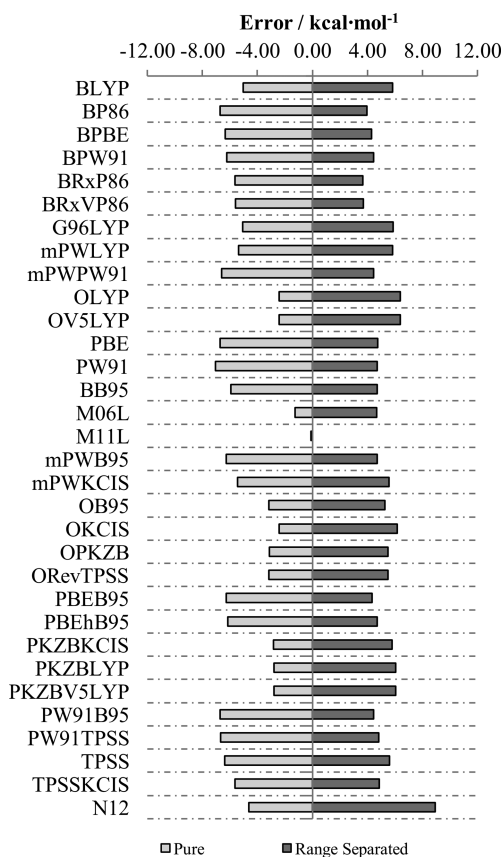


Figure 7. Signed error for the range separated version for a set of pure DFs from the study of the activation energy. The results are presented for the 6-311++G(2d,2p) basis set.

are the same from the pure DF. Out of all the screened HF exchange functionals, CAM-B3LYP performs best with a MUE of $1.42 \text{ kcal}\cdot\text{mol}^{-1}$.

We used dispersion corrections for 23 DFs available in Gaussian 09, with published dispersion parameters. For most cases, the dispersion correction does not improve the DF performance in our 15 atom model system, as can be seen in Table 5. The CAM-B3LYP and BHandHLYP functionals are

Table 5. MSE in the Activation Energy for Dispersion Corrected DFs Using the 6-311++G(2d,2p) Basis Set

DFs	no dispersion corrections	dispersion corrections	
		D3	D3-BJ
PBE	-6.74	-6.81	-7.50
TPSS	-6.38	-6.44	-7.36
BLYP	-5.04	-5.04	-6.88
B97		-4.25	-5.76
B3LYP	-2.31	-2.40	-3.85
B2PLYP	-2.58	-2.61	-3.36
BP86	-6.71	-6.75	-8.25
BPBE	-6.36	-6.37	-8.09
mPWLYP	-5.39	-5.47	-6.16
TPSSh	-4.87	-4.95	-5.76
OPBE		-4.67	-7.52
OLYP	-2.43	-3.64	-6.59
B3PW91	-3.27	-3.34	-4.73
PBE1PBE	-2.98	-3.05	-3.64
M06	-2.12	-2.16	-0.28
B1B95	-1.81	-1.83	-3.26
M06-L	-1.26	-1.25	-1.69
BMK	0.11	0.08	-1.22
mPWB1K	0.57	0.56	-0.01
CAM-B3LYP	1.42	1.38	0.79
BHandHLYP	2.84	2.79	1.47
LC- ω PBE	4.50	4.45	3.75
B2GPPLYP	-1.73	-1.74	-2.63
DSD-BLYP	-2.01	-2.02	-3.02

relevantly improved by the addition of Grimme's corrections with Becke–Johnson damping, with MSE of $0.79 \text{ kcal}\cdot\text{mol}^{-1}$ and $1.47 \text{ kcal}\cdot\text{mol}^{-1}$.

Despite no significant improvement is observed by employing both screened-exchange or dispersion corrections, we emphasize that our system under study is a small representative model and that for larger systems these corrections might be significant, even though past evidence is on our side.^{6,112–114} Overall, the BMK¹²¹ and M06-2X¹⁶² DFs show a good performance toward our CCSD(T)/CBS energies and are widely validated as good candidates for very good energy calculations in several other recent benchmark studies.^{41–43,46,49,50} The MN12-SX functional also shows overall good performance and should be considered as a proper candidate in this type of calculations.

DFT Performance in the Thiol–Disulfide Exchange Reaction. The final section of the paper presents an overall discussion of the DFs most suited to perform calculations for the thiol–disulfide exchange reaction. A quest for a density functional that may describe both thermodynamics and structure of a system is, ultimately, desired. Our benchmarking indicates that there is a clear prevalence of meta- or hybrid-density functionals with 40–50% HF exchange that perform best for our designed thiol–disulfide exchange model. The mPWB1K, mPW1N, mPW1K, and BB1K density functionals can be considered as good candidates to conduct calculations for this reaction; even though they were not the best candidates to reproduce the geometry of our 15 atom model, they are the most accurate to provide thermodynamics for thiol–disulfide exchange. Despite that M11-L, MN12-SX, and M06-2X show good results in all properties benchmarked in this study, they were not the best candidates to determine the PES for this model reaction.

CONCLUSIONS

Our study provides insight on the performance of a set of 92 density functionals characterizing thiol–disulfide exchange. This class of reactions is very important in biochemistry; therefore, the benchmarking of important thermodynamic and kinetic properties will allow for more accurate computational studies in large systems.

As found in other benchmarking studies, we have opted to design a small model (15 atoms) and use computationally demanding post-HF methods—MP2 and CCSD(T)—with correlation consistent basis sets (aug-cc-pVXZ, X = 2, 3, 4). These calculations provided us with accurate reference values, from the CBS extrapolation method of Varandas, which was employed to benchmark our set of density functionals.

Regarding the molecular geometry, several functionals reproduced well the geometry of the 15 atoms model. In particular M11-L, M06-2X, M06-HF, N12-SX, PBE1PBE, PBEh1PBE, and OHSE2PBE functionals produced geometries similar to MP2/aug-cc-pVTZ, with both the 6-31G(d) and the 6-31+G(d) basis sets. The hh-GGAs show very different results for both basis sets and were unable to reproduce the reference MP2/aug-cc-pVTZ geometry for the 6-31+G(d) basis set. Additionally, we highlight the less accurate performance of range-separated density functionals, in particular, for LC- ω PBE.

We selected 29 density functionals to reproduce the CCSD(T)/CBS PES along the reaction coordinate; our observations led us to conclude that no DF accurately reproduces both the energy and energy gradient of the $S_{\text{nuc}}-S_{\text{ctr}}$ attack. Nevertheless, h-GGA functionals showed the best

performance, in particular, for BHandH, mPW1N, mPW1K, and mPWB1K. DFs using 40–50% HF exchange result in an error for the reaction energy and PES in vacuum, often lower than $1.00 \text{ kcal}\cdot\text{mol}^{-1}$.

We tested 11 different basis sets—6-31+G(d,p), 6-31+G(2d,2p), 6-311G(d,p), 6-311G(2d,2p), 6-311G(2df,2p), 6-311G(2df,2pd) 6-311+G(df,p), 6-311+G(2d,2p), 6-311++G(df,p), 6-311++G(2d,2p), and TZVP—to evaluate the effect of the basis set in density functional performance toward the activation energy of thiol–disulfide exchange. Diffuse functions in heavy atoms may lead to a decrease of $0.10 \text{ kcal}\cdot\text{mol}^{-1}$ in relative activation energies for the reaction. The split-valence has a higher influence in the relative energy predicted, since the comparison between double and triple-split valences may lead to differences in relative energies of about $1.00 \text{ kcal}\cdot\text{mol}^{-1}$. As polarization functions are added to make the basis set more complete, relative activation energies from DFT calculations increase. While in the m-GGA set of density functionals these increments seem to provide more predictable differences, in most remaining cases the addition of f and p sets of functions to heavy atoms and hydrogens is more pronounced than the increasing of the d and p sets of functions. Overall, the M06-2X and BMK functionals provide the most accurate results against our CCSD(T)/CBS activation energies. The M11-L and MN12-SX functionals showed activation barriers with errors lower than $0.10 \text{ kcal}\cdot\text{mol}^{-1}$ from the CCSD(T)/CBS energies, for the typical 6-311++G(2d,2p) basis set (with MUEs of 0.05 and $0.02 \text{ kcal}\cdot\text{mol}^{-1}$, respectively). The calculations we performed for range separated and dispersion corrected functionals show no improvement, for all the functionals, except for the CAM-B3LYP functional, in which the MUE lowers from $1.42 \text{ kcal}\cdot\text{mol}^{-1}$ to $0.79 \text{ kcal}\cdot\text{mol}^{-1}$, with the Becke–Johnson damping. Dispersion in larger systems may be important but it will not be due to the thiol–disulfide exchange reaction itself. Instead, it will emanate from the many different molecular skeletons to which the thiols may be connected. This would be a problem of benchmarking intermolecular interactions, and not thiol–disulfide exchange. Therefore, we believe it is appropriate to say that dispersion does not have a meaningful role in the thiol–disulfide exchange reaction. Such corrections may turn out to be significant to accurately describe thermodynamic properties, among others, in larger systems. Despite the fact that the B3LYP functional does not show a good performance for any of the benchmarked properties, it shows a consistent average performance throughout the spectra of properties we have tested in our study.

Considering all aspects of the thiol–disulfide exchange reaction (geometry, PES, and activation energy) the mPWB1K, mPW1N, mPW1K, and BB1K density functionals are better suited to perform calculations for this reaction.

We believe that our current study shows a good systematic approach toward the benchmarking of specific chemical interactions that will hopefully prove to be useful in future computational studies concerning thiol–disulfide exchange reactions in complex systems.

ASSOCIATED CONTENT

Supporting Information

Linear transit scan for the $S_{\text{ctr}}-S_{\text{nuc}}$ reaction coordinate with the MP2 level of theory. Single-point energy calculations for MP2 and CCSD(T) levels of theory. CBS extrapolation schemes employed in the study. Rank of basis set from single-point MP2 calculations relative to CCSD(T)/CBS values. Benchmark of

the 92 DFs for the 6-311G++g(2d,2p) basis set. Single-point calculations for the basis set 6-31+G(d,p), 6-31+G(2d,2p), 6-311G(d,p), 6-311G(2d,2p), 6-311G(2df,p), 6-311G(2df,2pd), 6-311+G(df,p), 6-311++G(df,p), 6-311+G(2d,2p), 6-311++G(2d,2p), TZVP. Comparison of the relative energies for the 11 basis sets studies. MSE for the different integration grids for the basis set 6-311G(2df,2p), 6-311++G(df,p), and 6-311++G(2d,2p). MSE for the range separated version of a set of GGAs, for the basis set 6-311G(2df,2p), 6-311++G(df,p), and 6-311++G(2d,2p). MSE for the dispersion corrected DFs, for the basis set 6-311G(2df,2p), 6-311++G(df,p), and 6-311++G(2d,2p). Benchmark of optimization calculations for the 6-31G(d,p) and 6-31+G(d,p) basis set relative to the MP2/aug-cc-pVDZ optimized structure. MUE for the five equidistant steps in the S–S PES for the set of 30 DFs. This material is available free of charge via the Internet at <http://pubs.acs.org/>.

AUTHOR INFORMATION

Corresponding Author

*Email: mjramos@fc.up.pt

Author Contributions

R.P.P.N. performed all the calculations. A.J.C.V. helped in the discussion of theoretical aspects and results from CBS extrapolation schemes. P.A.F. and M.J.R. designed the computational experiments and supervised all the work. The manuscript was written through contributions of all authors. All authors have given approval to the final version of the manuscript.

Notes

The authors declare no competing financial interest.

ACKNOWLEDGMENTS

This work has been funded by FEDER/COMPETE and the Fundação para a Ciência e a Tecnologia (FCT) through projects EXCL/QEQ-COM/0394/2012 and PEST-C/EQB/LA0006/2013. R.P.P.N. further thanks the FCT for grant SFRH/BD/78397/2011. The support to A.J.C.V. by FCT under contracts PTDC/CEQ-COM3249/2012, PTDC/AAG-MAA/4657/2012, and SFRH/BPD/98132/2013 is also gratefully acknowledged.

REFERENCES

- (1) Rietsch, A.; Beckwith, J. The genetics of disulfide bond metabolism. *Annu. Rev. Genet.* **1998**, *32*, 163–184.
- (2) Wedemeyer, W. J.; Welker, E.; Narayan, M.; Scheraga, H. A. Disulfide bonds and protein folding. *Biochemistry* **2000**, *39*, 4207–4216.
- (3) Bošnjak, I.; Bojović, V.; Šegvić-Bubić, T.; Bielen, A. Occurrence of protein disulfide bonds in different domains of life: A comparison of proteins from the Protein Data Bank. *Protein Eng., Des. Sel.* **2014**, *27*, 65–72.
- (4) Sevier, C. S.; Kaiser, C. A. Formation and transfer of disulfide bonds in living cells. *Nat. Rev. Mol. Cell Biol.* **2002**, *3*, 836–847.
- (5) Hogg, P. J. Disulfide bonds as switches for protein function. *Trends Biochem. Sci.* **2003**, *28*, 210–214.
- (6) Fernandes, P. A.; Ramos, M. J. Theoretical insights into the mechanism for thiol/disulfide exchange. *Chem.—Eur. J.* **2004**, *10*, 257–266.
- (7) Rabenstein, D. L.; Weaver, K. H. Kinetics and equilibria of the thiol/disulfide exchange reactions of somatostatin with glutathione. *J. Org. Chem.* **1996**, *61*, 7391–7397.
- (8) Iozzi, M. F.; Helgaker, T.; Uggerud, E. Influence of external force on properties and reactivity of disulfide bonds. *J. Phys. Chem. A* **2011**, *115*, 2308–2315.

- (9) Rothwarf, D. M.; Scheraga, H. A. Equilibrium and kinetic constants for the thiol–disulfide interchange reaction between glutathione and dithiothreitol. *Proc. Natl. Acad. Sci. U.S.A.* **1992**, *89*, 7944–7948.

- (10) David, C.; Foley, S.; Mavon, C.; Enescu, M. Reductive unfolding of serum albumins uncovered by Raman spectroscopy. *Biopolymers* **2008**, *89*, 623–634.

- (11) Singh, R.; Whitesides, G. M. Thiol–disulfide interchange. In *Sulphur-Containing Functional Groups*; Patai, S.; Rappoport, Z., Eds.; John Wiley & Sons, Inc.: Chichester, U.K., 1993; Chapter 13, pp 633–658.

- (12) Edman, J. C.; Ellis, L.; Blacher, R. W.; Roth, R. A.; Rutter, W. J. Sequence of protein disulfide isomerase and implications of its relationship to thioredoxin. *Nature* **1985**, *317*, 267–270.

- (13) Carvalho, A. T. P.; Swart, M.; van Stralen, J. N. P.; Fernandes, P. A.; Ramos, M. J.; Bickelhaupt, F. M. Mechanism of thioredoxin-catalyzed disulfide reduction. Activation of the buried thiol and role of the variable active-site residues. *J. Phys. Chem. B* **2008**, *112*, 2511–2523.

- (14) Li, W.; Gräter, F. Atomistic evidence of how force dynamically regulates thiol/disulfide exchange. *J. Am. Chem. Soc.* **2010**, *132*, 16790–16795.

- (15) Levin, L.; Zelzion, E.; Nachliel, E.; Gutman, M.; Tsfadia, Y.; Einav, Y. A single disulfide bond disruption in the $\beta 3$ integrin subunit promotes thiol/disulfide exchange, a molecular dynamics study. *PLoS One* **2013**, *8*, e59175.

- (16) Thomas, L. H. The calculation of atomic fields. *Math. Proc. Cambridge Philos. Soc.* **1927**, *23*, 542–548.

- (17) Fermi, E. Un metodo statistico per la determinazione di alcune proprietà dell' atomo. *Rend. Accad. Naz. Lincei* **1927**, *602*–607.

- (18) Hohenberg, P.; Kohn, W. Inhomogeneous electron gas. *Phys. Rev.* **1964**, *136*, B864–B871.

- (19) Møller, C.; Plesset, M. S. Note on an approximation treatment for many-electron systems. *Phys. Rev.* **1934**, *46*, 618–622.

- (20) Maurice, D.; Head-Gordon, M. Analytical second derivatives for excited electronic states using the single excitation configuration interaction method: Theory and application to benzo[a]pyrene and chalcone. *Mol. Phys.* **1999**, *96*, 1533–1541.

- (21) Head-Gordon, M.; Rico, R. J.; Oumi, M.; Lee, T. J. A doubles correction to electronic excited states from configuration interaction in the space of single substitutions. *Chem. Phys. Lett.* **1994**, *219*, 21–29.

- (22) Purvis, G. D.; Bartlett, R. J. A full coupled-cluster singles and doubles model: The inclusion of disconnected triples. *J. Chem. Phys.* **1982**, *76*, 1910–1918.

- (23) Raghavachari, K.; Trucks, G. W.; Pople, J. A.; Head-Gordon, M. A fifth-order perturbation comparison of electron correlation theories. *Chem. Phys. Lett.* **1989**, *157*, 479–483.

- (24) Van Voorhis, T.; Head-Gordon, M. Two-body coupled cluster expansions. *J. Chem. Phys.* **2001**, *115*, 5033–5040.

- (25) Yanai, T.; Tew, D. P.; Handy, N. C. A new hybrid exchange–correlation functional using the Coulomb–attenuating method (CAM-B3LYP). *Chem. Phys. Lett.* **2004**, *393*, 51–57.

- (26) Heyd, J.; Scuseria, G. E. Efficient hybrid density functional calculations in solids: Assessment of the Heyd–Scuseria–Ernzerhof screened Coulomb hybrid functional. *J. Chem. Phys.* **2004**, *121*, 1187–1192.

- (27) Vydrov, O. A.; Scuseria, G. E.; Perdew, J. P. Tests of functionals for systems with fractional electron number. *J. Chem. Phys.* **2007**, *126*, 154109.

- (28) Vydrov, O. A.; Scuseria, G. E. Assessment of a long-range corrected hybrid functional. *J. Chem. Phys.* **2006**, *125*, 234109.

- (29) Vydrov, O. A.; Heyd, J.; Krukav, A. V.; Scuseria, G. E. Importance of short-range versus long-range Hartree–Fock exchange for the performance of hybrid density functionals. *J. Chem. Phys.* **2006**, *125*, 074106.

- (30) Chai, J.-D.; Head-Gordon, M. Systematic optimization of long-range corrected hybrid density functionals. *J. Chem. Phys.* **2008**, *128*, 084106.

- (31) Peverati, R.; Truhlar, D. G. Exchange-correlation functional with good accuracy for both structural and energetic properties while depending only on the density and its gradient. *J. Chem. Theor. Comput.* **2012**, *8*, 2310–2319.
- (32) Peverati, R.; Truhlar, D. G. An improved and broadly accurate local approximation to the exchange-correlation density functional: The MN12-L functional for electronic structure calculations in chemistry and physics. *Phys. Chem. Chem. Phys.* **2012**, *14*, 13171–13174.
- (33) Peverati, R.; Truhlar, D. G. Screened-exchange density functionals with broad accuracy for chemistry and solid-state physics. *Phys. Chem. Chem. Phys.* **2012**, *14*, 16187–16191.
- (34) Grimme, S. Semiempirical hybrid density functional with perturbative second-order correlation. *J. Chem. Phys.* **2006**, *124*, 034108.
- (35) Karton, A.; Tarnopolsky, A.; Lamère, J.-F.; Schatz, G. C.; Martin, J. M. L. Highly accurate first-principles benchmark data sets for the parametrization and validation of density functional and other approximate methods. Derivation of a robust, generally applicable, double-hybrid functional for thermochemistry and thermochemical kinetics. *J. Phys. Chem. A* **2008**, *112*, 12868–12886.
- (36) Schwabe, T.; Grimme, S. Towards chemical accuracy for the thermodynamics of large molecules: new hybrid density functionals including non-local correlation effects. *Phys. Chem. Chem. Phys.* **2006**, *8*, 4398–4401.
- (37) Kozuch, S.; Gruzman, D.; Martin, J. M. L. DSD-BLYP: A general purpose double hybrid density functional including spin component scaling and dispersion correction. *J. Phys. Chem. C* **2010**, *114*, 20801–20808.
- (38) Zhang, I. Y.; Luo, Y.; Xu, X. XYG3s: Speedup of the XYG3 fifth-rung density functional with scaling-all-correlation method. *J. Chem. Phys.* **2010**, *132*, 194105.
- (39) Zhang, I. Y.; Luo, Y.; Xu, X. Basis set dependence of the doubly hybrid XYG3 functional. *J. Chem. Phys.* **2010**, *133*, 104105.
- (40) Zhang, Y.; Xu, X.; Goddard, W. A. Doubly hybrid density functional for accurate descriptions of nonbond interactions, thermochemistry, and thermochemical kinetics. *Proc. Natl. Acad. Sci. U.S.A.* **2009**, *106*, 4963–4968.
- (41) Ribeiro, A. n. J. M.; Ramos, M. J.; Fernandes, P. A. Benchmarking of DFT functionals for the hydrolysis of phosphodiester bonds. *J. Chem. Theor. Comput.* **2010**, *6*, 2281–2292.
- (42) Goerigk, L.; Grimme, S. A thorough benchmark of density functional methods for general main group thermochemistry, kinetics, and noncovalent interactions. *Phys. Chem. Chem. Phys.* **2011**, *13*, 6670–6688.
- (43) Brás, N. F.; Perez, M. A. S.; Fernandes, P. A.; Silva, P. J.; Ramos, M. J. Accuracy of density functionals in the prediction of electronic proton affinities of amino acid side chains. *J. Chem. Theor. Comput.* **2011**, *7*, 3898–3908.
- (44) Sousa, S. F.; Pinto, G. R. P.; Ribeiro, A. J. M.; Coimbra, J. T. S.; Fernandes, P. A.; Ramos, M. J. Comparative analysis of the performance of commonly available density functionals in the determination of geometrical parameters for copper complexes. *J. Comput. Chem.* **2013**, *34*, 2079–2090.
- (45) Goerigk, L.; Grimme, S. A general database for main group thermochemistry, kinetics, and noncovalent interactions—Assessment of common and reparameterized (meta-)GGA density functionals. *J. Chem. Theor. Comput.* **2010**, *6*, 107–126.
- (46) Peverati, R.; Truhlar, D. G. Quest for a universal density functional: the accuracy of density functionals across a broad spectrum of databases in chemistry and physics. *Philos. Trans. R. Soc., A* **2014**, *372*.
- (47) Ondarza, R. Enzyme regulation by biological disulfides. *Biosci. Rep.* **1989**, *9*, 593–604.
- (48) Fass, D. Disulfide bonding in protein biophysics. *Annu. Rev. Biophys.* **2012**, *41*, 63–79.
- (49) Zhao, Y.; Truhlar, D. G. Density functional theory for reaction energies: Test of meta and hybrid meta functionals, range-separated functionals, and other high-performance functionals. *J. Chem. Theor. Comput.* **2011**, *7*, 669–676.
- (50) Dumont, É.; Laurent, A. D.; Assfeld, X.; Jacquemin, D. Performances of recently-proposed functionals for describing disulfide radical anions and similar systems. *Chem. Phys. Lett.* **2011**, *501*, 245–251.
- (51) Grimme, S. Semiempirical GGA-type density functional constructed with a long-range dispersion correction. *J. Comput. Chem.* **2006**, *27*, 1787–1799.
- (52) Grimme, S.; Antony, J.; Ehrlich, S.; Krieg, H. A consistent and accurate ab initio parametrization of density functional dispersion correction (DFT-D) for the 94 elements H-Pu. *J. Chem. Phys.* **2010**, *132*.
- (53) Grimme, S.; Ehrlich, S.; Goerigk, L. Effect of the damping function in dispersion corrected density functional theory. *J. Comput. Chem.* **2011**, *32*, 1456–1465.
- (54) Becke, A. D.; Johnson, E. R. Exchange-hole dipole moment and the dispersion interaction. *J. Chem. Phys.* **2005**, *122*.
- (55) Bartlett, R. J.; Purvis, G. D. Many-body perturbation-theory, coupled-pair many-electron theory, and importance of quadruple excitations for correlation problem. *Int. J. Quantum Chem.* **1978**, *14*, 561–581.
- (56) Pople, J. A.; Krishnan, R.; Schlegel, H. B.; Binkley, J. S. Electron correlation theories and their application to study of simple reaction potential surfaces. *Int. J. Quantum Chem.* **1978**, *14*, 545–560.
- (57) Čížek, J. *Correlation Effects in Atoms and Molecules*; Wiley Interscience: New York, 1969; Vol. 14.
- (58) Pople, J. A.; Head-Gordon, M.; Raghavachari, K. Quadratic configuration-interaction—A general technique for determining electron correlation energies. *J. Chem. Phys.* **1987**, *87*, 5968–5975.
- (59) Scuseria, G. E.; Janssen, C. L.; Schaefer, H. F. An efficient reformulation of the closed-shell coupled cluster single and double excitation (CCSD) equations. *J. Chem. Phys.* **1988**, *89*, 7382–7387.
- (60) Scuseria, G. E.; Schaefer, H. F. Is coupled cluster singles and doubles (CCSD) more computationally intensive than quadratic configuration-interaction (QCISD). *J. Chem. Phys.* **1989**, *90*, 3700–3703.
- (61) Helgaker, T.; Klopper, W.; Koch, H.; Noga, J. Basis-set convergence of correlated calculations on water. *J. Chem. Phys.* **1997**, *106*, 9639–9646.
- (62) Halkier, A.; Helgaker, T.; Jørgensen, P.; Klopper, W.; Koch, H.; Olsen, J.; Wilson, A. K. Basis-set convergence in correlated calculations on Ne, N₂, and H₂O. *Chem. Phys. Lett.* **1998**, *286*, 243–252.
- (63) Truhlar, D. G. Basis-set extrapolation. *Chem. Phys. Lett.* **1998**, *294*, 45–48.
- (64) Zhao, Y.; Truhlar, D. G. Infinite-basis calculations of binding energies for the hydrogen bonded and stacked tetramers of formic acid and formamide and their use for validation of hybrid DFT and ab initio methods. *J. Phys. Chem. A* **2005**, *109*, 6624–6627.
- (65) Varandas, A. J. C. Extrapolating to the one-electron basis-set limit in electronic structure calculations. *J. Chem. Phys.* **2007**, *126*, 244105.
- (66) Angelucci, F.; Dimastrogiovanni, D.; Boumis, G.; Brunori, M.; Miele, A. E.; Saccoccia, F.; Bellelli, A. Mapping the catalytic cycle of *Schistosoma mansoni* thioredoxin glutathione reductase by X-ray crystallography. *J. Biol. Chem.* **2010**, *285*, 32557–32567.
- (67) Frisch, M. J.; Trucks, G. W.; Schlegel, H. B.; Scuseria, G. E.; Robb, M. A.; Cheeseman, J. R.; Scalmani, G.; Barone, V.; Mennucci, B.; Petersson, G. A.; Nakatsuji, H.; Caricato, M.; Li, X.; Hratchian, H. P.; Izmaylov, A. F.; Bloino, J.; Zheng, G.; Sonnenberg, J. L.; Hada, M.; Ehara, M.; Toyota, K.; Fukuda, R.; Hasegawa, J.; Ishida, M.; Nakajima, T.; Honda, Y.; Kitao, O.; Nakai, H.; Vreven, T.; Montgomery, J. A., Jr.; Peralta, J. E.; Ogliaro, F.; Bearpark, M.; Heyd, J. J.; Brothers, E.; Kudin, K. N.; Staroverov, V. N.; Kobayashi, R.; Normand, J.; Raghavachari, K.; Rendell, A.; Burant, J. C.; Iyengar, S. S.; Tomasi, J.; Cossi, M.; Rega, N.; Millam, J. M.; Klene, M.; Knox, J. E.; Cross, J. B.; Bakken, V.; Adamo, C.; Jaramillo, J.; Gomperts, R.; Stratmann, R. E.; Yazyev, O.; Austin, A. J.; Cammi, R.; Pomelli, C.; Ochterski, J. W.; Martin, R. L.; Morokuma, K.; Zakrzewski, V. G.; Voth, G. A.; Salvador,

P.; Dannenberg, J. J.; Dapprich, S.; Daniels, A. D.; Farkas, Ö.; Foresman, J. B.; Ortiz, J. V.; Cioslowski, J.; Fox, D. J. *Gaussian 09*, Revision D.01; Gaussian, Inc.: Wallingford, CT, 2009.

(68) Dunning, T. H. Gaussian basis sets for use in correlated molecular calculations. I. The atoms boron through neon and hydrogen. *J. Chem. Phys.* **1989**, *90*, 1007–1023.

(69) Kendall, R. A.; Dunning, T. H.; Harrison, R. J. Electron affinities of the first-row atoms revisited. Systematic basis sets and wave functions. *J. Chem. Phys.* **1992**, *96*, 6796–6806.

(70) Woon, D. E.; Dunning, T. H. Gaussian basis sets for use in correlated molecular calculations. III. The atoms aluminum through argon. *J. Chem. Phys.* **1993**, *98*, 1358–1371.

(71) Barone, V.; Cossi, M. Quantum calculation of molecular energies and energy gradients in solution by a conductor solvent model. *J. Phys. Chem. A* **1998**, *102*, 1995–2001.

(72) Cossi, M.; Rega, N.; Scalmani, G.; Barone, V. Energies, structures, and electronic properties of molecules in solution with the C-PCM solvation model. *J. Comput. Chem.* **2003**, *24*, 669–681.

(73) Hobza, P.; Sponer, J. Toward true DNA base-stacking energies: MP2, CCSD(T), and complete basis set calculations. *J. Am. Chem. Soc.* **2002**, *124*, 11802–11808.

(74) Jurecka, P.; Hobza, P. On the convergence of the (Delta E-CCSD(T)-Delta E-MP2) term for complexes with multiple H-bonds. *Chem. Phys. Lett.* **2002**, *365*, 89–94.

(75) Daabkowska, I.; Jurecka, P.; Hobza, P. On geometries of stacked and H-bonded nucleic acid base pairs determined at various DFT, MP2, and CCSD(T) levels up to the CCSD(T)/complete basis set limit level. *J. Chem. Phys.* **2005**, *122*.

(76) Ditchfie, R.; Hehre, W. J.; Pople, J. A. Self-consistent molecular-orbital methods. 9. Extended Gaussian-type basis for molecular-orbital studies of organic molecules. *J. Chem. Phys.* **1971**, *54*, 724.

(77) Hehre, W. J.; Ditchfie, R.; Pople, J. A. Self-consistent molecular-orbital methods. 12. Further extensions of Gaussian-type basis sets for use in molecular-orbital studies of organic molecules. *J. Chem. Phys.* **1972**, *56*, 2257.

(78) Hariharan, P. C.; Pople, J. A. The influence of polarization functions on molecular orbital hydrogenation energies. *Theor. Chim. Acta* **1973**, *28*, 213–222.

(79) Hariharan, P. C.; Pople, J. A. Accuracy of AH n equilibrium geometries by single determinant molecular orbital theory. *Mol. Phys.* **1974**, *27*, 209–214.

(80) Gordon, M. S. The isomers of silacyclopropane. *Chem. Phys. Lett.* **1980**, *76*, 163–168.

(81) Francl, M. M.; Pietro, W. J.; Hehre, W. J.; Binkley, J. S.; Gordon, M. S.; Defrees, D. J.; Pople, J. A. Self-consistent molecular-orbital methods. 23. A polarization-type basis set for 2nd-row elements. *J. Chem. Phys.* **1982**, *77*, 3654–3665.

(82) Clark, T.; Chandrasekhar, J.; Spitznagel, G. W.; Schleyer, P. V. R. Efficient diffuse function-augmented basis sets for anion calculations. III. The 3-21+G basis set for first-row elements, Li–F. *J. Comput. Chem.* **1983**, *4*, 294–301.

(83) Bras, N. F.; Moura-Tamames, S. A.; Fernandes, P. A.; Ramos, M. J. Mechanistic studies on the formation of glycosidase-substrate and glycosidase-inhibitor covalent intermediates. *J. Comput. Chem.* **2008**, *29*, 2565–2574.

(84) Oliveira, E. F.; Cerqueira, N. M. F. S. A.; Fernandes, P. A.; Ramos, M. J. Mechanism of formation of the internal aldimine in pyridoxal 5'-phosphate-dependent enzymes. *J. Am. Chem. Soc.* **2011**, *133*, 15496–15505.

(85) Ribeiro, A. J. M.; Ramos, M. J.; Fernandes, P. A. The catalytic mechanism of HIV-1 integrase for DNA 3'-end processing established by QM/MM calculations. *J. Am. Chem. Soc.* **2012**, *134*, 13436–13447.

(86) Gesto, D. S.; Cerqueira, N. M. F. S. A.; Fernandes, P. A.; Ramos, M. J. Unraveling the enigmatic mechanism of L-asparaginase II with QM/QM calculations. *J. Am. Chem. Soc.* **2013**, *135*, 7146–7158.

(87) Maranzana, A.; Giordana, A.; Indarto, A.; Tonachini, G.; Barone, V.; Causa, M.; Pavone, M. Density functional theory study of the interaction of vinyl radical, ethyne, and ethene with benzene, aimed to

define an affordable computational level to investigate stability trends in large van der Waals complexes. *J. Chem. Phys.* **2013**, *139*.

(88) Sekharan, S.; Mooney, V. L.; Rivalta, I.; Kazmi, M. A.; Neitz, M.; Neitz, J.; Sakmar, T. P.; Yan, E. C. Y.; Batista, V. S. Spectral tuning of ultraviolet cone pigments: An interhelical lock mechanism. *J. Am. Chem. Soc.* **2013**, *135*, 19064–19067.

(89) Becke, A. D. Density-functional exchange-energy approximation with correct asymptotic behavior. *Phys. Rev. A* **1988**, *38*, 3098–3100.

(90) Lee, C. T.; Yang, W. T.; Parr, R. G. Development of the Colle–Salvetti correlation-energy formula into a functional of the electron density. *Phys. Rev. B* **1988**, *37*, 785–789.

(91) Becke, A. D. Density-functional thermochemistry. 4. A new dynamical correlation functional and implications for exact-exchange mixing. *J. Chem. Phys.* **1996**, *104*, 1040–1046.

(92) Varandas, A. J. C. Accurate determination of the reaction course in HY2 (sic) Y + YH (Y = O, S): Detailed analysis of the covalent- to hydrogen-bonding transition. *J. Phys. Chem. A* **2013**, *117*, 7393–7407.

(93) Varandas, A. J. C. Odd-hydrogen: An account on electronic structure, kinetics and role of water in mediating reactions with atmospheric ozone. Just a catalyst or far beyond? *Int. J. Quantum Chem.* **2014**, *118*, 1327–1349.

(94) Viegas, L. P.; Varandas, A. J. C. Coupled-cluster reaction barriers of HO₂ + H₂O + O₃: An application of the coupled-cluster//Kohn–Sham density functional theory model chemistry. *J. Comput. Chem.* **2014**, *35*, 507–517.

(95) Mclean, A. D.; Chandler, G. S. Contracted Gaussian-basis sets for molecular calculations. 1. 2nd row atoms, Z = 11–18. *J. Chem. Phys.* **1980**, *72*, 5639–5648.

(96) Krishnan, R.; Binkley, J. S.; Seeger, R.; Pople, J. A. Self-consistent molecular-orbital methods. 20. Basis set for correlated wavefunctions. *J. Chem. Phys.* **1980**, *72*, 650–654.

(97) Frisch, M. J.; Pople, J. A.; Binkley, J. S. Self-consistent molecular-orbital methods. 25. Supplementary functions for Gaussian-basis sets. *J. Chem. Phys.* **1984**, *80*, 3265–3269.

(98) Schäfer, A.; Huber, C.; Ahlrichs, R. Fully optimized contracted Gaussian basis sets of triple zeta valence quality for atoms Li to Kr. *J. Chem. Phys.* **1994**, *100*, 5829–5835.

(99) Wheeler, S. E.; Houk, K. N. Integration grid errors for meta-GGA-predicted reaction energies: Origin of grid errors for the M06 Suite of functionals. *J. Chem. Theor. Comput.* **2010**, *6*, 395–404.

(100) Iikura, H.; Tsuneda, T.; Yanai, T.; Hirao, K. A long-range correction scheme for generalized-gradient-approximation exchange functionals. *J. Chem. Phys.* **2001**, *115*, 3540–3544.

(101) Goerigk, L.; Reimers, J. R. Efficient methods for the quantum chemical treatment of protein structures: The effects of london-dispersion and basis-set incompleteness on peptide and water-cluster geometries. *J. Chem. Theor. Comput.* **2013**, *9*, 3240–3251.

(102) Sousa, S. F.; Fernandes, P. A.; Ramos, M. J. General performance of density functionals. *J. Phys. Chem. A* **2007**, *111*, 10439–10452.

(103) Minenkov, Y.; Singstad, A.; Occhipinti, G.; Jensen, V. R. The accuracy of DFT-optimized geometries of functional transition metal compounds: A validation study of catalysts for olefin metathesis and other reactions in the homogeneous phase. *Dalton Trans.* **2012**, *41*, 5526–5541.

(104) Kozuch, S.; Martin, J. M. L. Halogen bonds: Benchmarks and theoretical analysis. *J. Chem. Theor. Comput.* **2013**, *9*, 1918–1931.

(105) Valdes, H.; Pluhackova, K.; Pitonak, M.; Rezac, J.; Hobza, P. Benchmark database on isolated small peptides containing an aromatic side chain: Comparison between wave function and density functional theory methods and empirical force field. *Phys. Chem. Chem. Phys.* **2008**, *10*, 2747–2757.

(106) Valdes, H.; Pluhackova, K.; Hobza, P. Phenylalanyl-glycyl-phenylalanine tripeptide: A model system for aromatic–aromatic side chain interactions in proteins. *J. Chem. Theor. Comput.* **2009**, *5*, 2248–2256.

(107) Kruse, H.; Goerigk, L.; Grimme, S. Why the standard B3LYP/6-31G* model chemistry should not be used in DFT calculations of

molecular thermochemistry: Understanding and correcting the problem. *J. Org. Chem.* **2012**, *77*, 10824–10834.

(108) Carvalho, A. T. P.; Fernandes, P. A.; Ramos, M. J. Determination of the ΔpK_a between the active site cysteines of thioredoxin and DsbA. *J. Comput. Chem.* **2006**, *27*, 966–975.

(109) Carvalho, A. T. P.; Fernandes, P. A.; Ramos, M. J. Theoretical study of the unusual protonation properties of the active site cysteines in thioredoxin. *J. Phys. Chem. B* **2006**, *110*, 5758–5761.

(110) Carvalho, A. P.; Fernandes, P. A.; Ramos, M. J. Similarities and differences in the thioredoxin superfamily. *Prog. Biophys. Mol. Biol.* **2006**, *91*, 229–248.

(111) Carvalho, A. T. P.; Fernandes, P. A.; Swart, M.; van Stralen, J. N. P.; Bickelhaupt, F. M.; Ramos, M. J. Role of the variable active site residues in the function of thioredoxin family oxidoreductases. *J. Comput. Chem.* **2009**, *30*, 710–724.

(112) Wiita, A. P.; Ainavarapu, R. K.; Huang, H. H.; Fernandez, J. M. Force-dependent chemical kinetics of disulfide bond reduction observed with single-molecule techniques. *Proc. Natl. Acad. Sci. U.S.A.* **2006**, *103*, 7222–7227.

(113) Wiita, A. P.; Perez-Jimenez, R.; Walther, K. A.; Grater, F.; Berne, B. J.; Holmgren, A.; Sanchez-Ruiz, J. M.; Fernandez, J. M. Probing the chemistry of thioredoxin catalysis with force. *Nature* **2007**, *450*, 124.

(114) Alegre-Cebollada, J.; Perez-Jimenez, R.; Kosuri, P.; Fernandez, J. M. Single-molecule Force Spectroscopy Approach to Enzyme Catalysis. *J. Biol. Chem.* **2010**, *285*, 18961–18966.

(115) Perdew, J. P. *Electronic Structure of Solids '91*; Akademie Verlag: Berlin, 1991; Vol. 11.

(116) Perdew, J. P.; Chevary, J. A.; Vosko, S. H.; Jackson, K. A.; Pederson, M. R.; Singh, D. J.; Fiolhais, C. Atoms, molecules, solids, and surfaces - applications of the generalized gradient approximation for exchange and correlation. *Phys. Rev. B* **1992**, *46*, 6671–6687.

(117) Perdew, J. P.; Chevary, J. A.; Vosko, S. H.; Jackson, K. A.; Pederson, M. R.; Singh, D. J.; Fiolhais, C. Erratum: Atoms, molecules, solids, and surfaces—Applications of the generalized gradient approximation for exchange and correlation (Vol 46, Pg 6671, 1992). *Phys. Rev. B* **1993**, *48*, 4978–4978.

(118) Perdew, J. P.; Burke, K.; Wang, Y. Generalized gradient approximation for the exchange-correlation hole of a many-electron system. *Phys. Rev. B* **1996**, *54*, 16533–16539.

(119) Burke, K.; Perdew, J. P.; Wang, Y. *Electronic Density Functional Theory: Recent Progress and New Directions*; Springer Plenum: New York, 1998.

(120) Adamo, C.; Barone, V. Exchange functionals with improved long-range behavior and adiabatic connection methods without adjustable parameters: The mPW and mPW1PW models. *J. Chem. Phys.* **1998**, *108*, 664–675.

(121) Boese, A. D.; Martin, J. M. L. Development of density functionals for thermochemical kinetics. *J. Chem. Phys.* **2004**, *121*, 3405–3416.

(122) Zhao, Y.; Lynch, B. J.; Truhlar, D. G. Development and assessment of a new hybrid density functional model for thermochemical kinetics. *J. Phys. Chem. A* **2004**, *108*, 2715–2719.

(123) Viegas, L. P.; Branco, A.; Varandas, A. J. C. How well can Kohn–Sham DFT describe the HO₂ + O₃ reaction? *J. Chem. Theor. Comput.* **2010**, *6*, 2751–2761.

(124) Kohn, W.; Sham, L. J. Self-consistent equations including exchange and correlation effects. *Phys. Rev.* **1965**, *140*, A1133–A1138.

(125) Slater, J. C. *The Self-Consistent Field for Molecular and Solids, Quantum Theory of Molecular and Solids*; McGraw-Hill: New York, 1974; Vol. 4.

(126) Vosko, S. H.; Wilk, L.; Nusair, M. Accurate spin-dependent electron liquid correlation energies for local spin-density calculations—A critical analysis. *Can. J. Phys.* **1980**, *58*, 1200–1211.

(127) Perdew, J. P.; Zunger, A. Self-interaction correction to density-functional approximations for many-electron systems. *Phys. Rev. B* **1981**, *23*, 5048–5079.

(128) Perdew, J. P. Density-functional approximation for the correlation-energy of the inhomogeneous electron-gas. *Phys. Rev. B* **1986**, *33*, 8822–8824.

(129) Becke, A. D.; Roussel, M. R. Exchange holes in inhomogeneous systems—A coordinate-space model. *Phys. Rev. A* **1989**, *39*, 3761–3767.

(130) Miehlich, B.; Savin, A.; Stoll, H.; Preuss, H. Results obtained with the correlation-energy density functionals of Becke and Lee, Yang and Parr. *Chem. Phys. Lett.* **1989**, *157*, 200–206.

(131) Devlin, F. J.; Finley, J. W.; Stephens, P. J.; Frisch, M. J. Ab initio calculation of vibrational absorption and circular dichroism spectra using density functional force fields: A comparison of local, nonlocal, and hybrid density functionals. *J. Phys. Chem.* **1995**, *99*, 16883–16902.

(132) Gill, P. M. W. A new gradient-corrected exchange functional. *Mol. Phys.* **1996**, *89*, 433–445.

(133) Perdew, J. P.; Burke, K.; Ernzerhof, M. Generalized gradient approximation made simple. *Phys. Rev. Lett.* **1996**, *77*, 3865–3868.

(134) Adamo, C.; Barone, V. Toward reliable adiabatic connection models free from adjustable parameters. *Chem. Phys. Lett.* **1997**, *274*, 242–250.

(135) Becke, A. D. Density-functional thermochemistry. V. Systematic optimization of exchange-correlation functionals. *J. Chem. Phys.* **1997**, *107*, 8554–8560.

(136) Perdew, J. P.; Burke, K.; Ernzerhof, M. Erratum: Generalized gradient approximation made simple (vol 77, pg 3865, 1996). *Phys. Rev. Lett.* **1997**, *78*, 1396–1396.

(137) Adamo, C.; Barone, V. Implementation and validation of the Lacks–Gordon exchange functional in conventional density functional and adiabatic connection methods. *J. Comput. Chem.* **1998**, *19*, 418–429.

(138) Ernzerhof, M.; Perdew, J. P. Generalized gradient approximation to the angle- and system-averaged exchange hole. *J. Chem. Phys.* **1998**, *109*, 3313–3320.

(139) Hamprecht, F. A.; Cohen, A. J.; Tozer, D. J.; Handy, N. C. Development and assessment of new exchange-correlation functionals. *J. Chem. Phys.* **1998**, *109*, 6264–6271.

(140) Rey, J.; Savin, A. Virtual space level shifting and correlation energies. *Int. J. Quantum Chem.* **1998**, *69*, 581–590.

(141) Schmider, H. L.; Becke, A. D. Optimized density functionals from the extended G2 test set. *J. Chem. Phys.* **1998**, *108*, 9624–9631.

(142) Van Voorhis, T.; Scuseria, G. E. A novel form for the exchange-correlation energy functional. *J. Chem. Phys.* **1998**, *109*, 400–410.

(143) Adamo, C.; Barone, V. Toward reliable density functional methods without adjustable parameters: The PBE0 model. *J. Chem. Phys.* **1999**, *110*, 6158–6170.

(144) Perdew, J. P.; Kurth, S.; Zupan, A.; Blaha, P. Accurate density functional with correct formal properties: A step beyond the generalized gradient approximation. *Phys. Rev. Lett.* **1999**, *82*, 2544–2547.

(145) Lynch, B. J.; Fast, P. L.; Harris, M.; Truhlar, D. G. Adiabatic Connection for Kinetics. *J. Phys. Chem. A* **2000**, *104*, 4811–4815.

(146) Handy, N. C.; Cohen, A. J. Left-right correlation energy. *Mol. Phys.* **2001**, *99*, 403–412.

(147) Hoe, W. M.; Cohen, A. J.; Handy, N. C. Assessment of a new local exchange functional OPTX. *Chem. Phys. Lett.* **2001**, *341*, 319–328.

(148) Wilson, P. J.; Bradley, T. J.; Tozer, D. J. Hybrid exchange-correlation functional determined from thermochemical data and ab initio potentials. *J. Chem. Phys.* **2001**, *115*, 9233–9242.

(149) Kormos, B. L.; Cramer, C. J. Adiabatic connection method for X⁻ + RX nucleophilic substitution reactions (X = F, Cl). *J. Phys. Org. Chem.* **2002**, *15*, 712–720.

(150) Toulouse, J.; Savin, A.; Adamo, C. Validation and assessment of an accurate approach to the correlation problem in density functional theory: The Kriger–Chen–Iafate–Savin model. *J. Chem. Phys.* **2002**, *117*, 10465–10473.

(151) Boese, A. D.; Martin, J. M. L.; Handy, N. C. The role of the basis set: Assessing density functional theory. *J. Chem. Phys.* **2003**, *119*, 3005–3014.

(152) Lynch, B. J.; Zhao, Y.; Truhlar, D. G. Effectiveness of diffuse basis functions for calculating relative energies by density functional theory. *J. Phys. Chem. A* **2003**, *107*, 1384–1388.

(153) Tao, J. M.; Perdew, J. P.; Staroverov, V. N.; Scuseria, G. E. Climbing the density functional ladder: Nonempirical meta-generalized gradient approximation designed for molecules and solids. *Phys. Rev. Lett.* **2003**, *91*.

(154) Xu, X.; Goddard, W. A. The X3LYP extended density functional for accurate descriptions of nonbond interactions, spin states, and thermochemical properties. *Proc. Natl. Acad. Sci. U.S.A.* **2004**, *101*, 2673–2677.

(155) Zhao, Y.; Truhlar, D. G. Hybrid meta density functional theory methods for thermochemistry, thermochemical kinetics, and non-covalent interactions: The MPW1B95 and MPWB1K models and comparative assessments for hydrogen bonding and van der Waals interactions. *J. Phys. Chem. A* **2004**, *108*, 6908–6918.

(156) Dahlke, E. E.; Truhlar, D. G. Improved density functionals for water. *J. Phys. Chem. B* **2005**, *109*, 15677–15683.

(157) Zhao, Y.; González-García, N.; Truhlar, D. G. Benchmark database of barrier heights for heavy atom transfer, nucleophilic substitution, association, and unimolecular reactions and its use to test theoretical methods. *J. Phys. Chem. A* **2005**, *109*, 2012–2018.

(158) Zhao, Y.; Truhlar, D. G. Benchmark databases for nonbonded interactions and their use to test density functional theory. *J. Chem. Theor. Comput.* **2005**, *1*, 415–432.

(159) Zhao, Y.; Schultz, N. E.; Truhlar, D. G. Design of density functionals by combining the method of constraint satisfaction with parametrization for thermochemistry, thermochemical kinetics, and noncovalent interactions. *J. Chem. Theor. Comput.* **2006**, *2*, 364–382.

(160) Zhao, Y.; Truhlar, D. G. Density functional for spectroscopy: No long-range self-interaction error, good performance for Rydberg and charge-transfer states, and better performance on average than B3LYP for ground states. *J. Phys. Chem. A* **2006**, *110*, 13126–13130.

(161) Zhao, Y.; Truhlar, D. G. Comparative DFT study of van der Waals complexes: Rare-gas dimers, alkaline-earth dimers, zinc dimer, and zinc–rare-gas dimers. *J. Phys. Chem. A* **2006**, *110*, 5121–5129.

(162) Zhao, Y.; Truhlar, D. The M06 suite of density functionals for main group thermochemistry, thermochemical kinetics, noncovalent interactions, excited states, and transition elements: Two new functionals and systematic testing of four M06-class functionals and 12 other functionals. *Theor. Chem. Acc.* **2008**, *120*, 215–241.

(163) Perdew, J. P.; Ruzsinszky, A.; Csonka, G. I.; Constantin, L. A.; Sun, J. W. Workhorse semilocal density functional for condensed matter physics and quantum chemistry. *Phys. Rev. Lett.* **2009**, *103*.

(164) Peverati, R.; Truhlar, D. G. Communication: A global hybrid generalized gradient approximation to the exchange-correlation functional that satisfies the second-order density-gradient constraint and has broad applicability in chemistry. *J. Chem. Phys.* **2011**, *135*.

(165) Austin, A.; Petersson, G. A.; Frisch, M. J.; Dobek, F. J.; Scalmani, G.; Throssell, K. A Density Functional with Spherical Atom Dispersion Terms. *J. Chem. Theor. Comput.* **2012**, *8*, 4989–5007.

(166) Peverati, R.; Truhlar, D. G. M11-L: A local density functional that provides improved accuracy for electronic structure calculations in chemistry and physics. *J. Phys. Chem. Lett.* **2012**, *3*, 117–124.